AGU ADVANCING EARTH AND SPACE SCIENCES

Reviews of Geophysics

REVIEW ARTICLE
10.1029/2025RG000903

Key Points:

- Studies regarding the role of bubbles on air-sea gas exchange over the past decades are reviewed
- Bubble-mediated gas transfer is strongly nonlinear, solubility-dependent, and asymmetric; its role in carbon dioxide flux is debated
- Key knowledge gaps include upper ocean bubble dynamics, sensitivity to solubility, and the scaling from laboratory to field

Supporting Information:

Supporting Information may be found in the online version of this article.

Correspondence to:

Y. Dong,
ydong@geomar.de

Citation:

Dong, Y., Jähne, B., Woolf, D. K., Krall, K. E., Yang, M., Czerski, H., et al. (2026). The role of bubbles in air-sea gas exchange: A critical review. *Reviews of Geophysics*, *64*, e2025RG000903. https://doi.org/10.1029/2025RG000903

Received 14 AUG 2025
Accepted 10 JUN 2026

Author Contributions:

Conceptualization: Yuanxu Dong, Bernd Jähne, David K. Woolf, Christa A. Marandino
Data curation: Yuanxu Dong
Formal analysis: Yuanxu Dong, David K. Woolf
Funding acquisition: Yuanxu Dong, Bernd Jähne, Christa A. Marandino
Methodology: Yuanxu Dong, Bernd Jähne, David K. Woolf, Kerstin E. Krall, Mingxi Yang, Helen Czerski, Junhong Liang, Ian M. Brooks, David T. Ho, Dariia Atamanchuk, Christa A. Marandino
Project administration: Bernd Jähne, Christa A. Marandino
Resources: Yuanxu Dong, Bernd Jähne, David K. Woolf, Kerstin E. Krall, Mingxi Yang, Christa A. Marandino

The Role of Bubbles in Air-Sea Gas Exchange: A Critical Review

Yuanxu Dong[1,2,3], Bernd Jähne[2,4], David K. Woolf[5], Kerstin E. Krall[2], Mingxi Yang[6], Helen Czerski[7], Junhong Liang[8,9], Ian M. Brooks[10], Craig L. McNeil[11], Rik Wanninkhof[12], David T. Ho[13], Dariia Atamanchuk[14], and Christa A. Marandino[1]

[1]Research Division 2-Biogeochemistry, GEOMAR Helmholtz Centre for Ocean Research Kiel, Kiel, Germany, [2]Institute of Environmental Physics, Heidelberg University, Heidelberg, Germany, [3]Now at Laboratoire de Météorologie Dynamique, LMD-IPSL, École Normale Supérieure, Université PSL, École Polytechnique, Institut Polytechnique de Paris, Sorbonne Université, CNRS, Paris, France, [4]Interdisciplinary Center for Scientific Computing (IWR), Heidelberg University, Heidelberg, Germany, [5]Institute of Life and Earth Sciences, Heriot-Watt University, Stromness, UK, [6]Plymouth Marine Laboratory, Plymouth, UK, [7]Department of Mechanical Engineering, University College London, London, UK, [8]Department of Earth, Ocean and Atmospheric Science, Florida State University, Tallahassee, FL, USA, [9]Center for Ocean-Atmospheric Prediction Studies, Florida State University, Tallahassee, FL, USA, [10]School of Earth and Environment, University of Leeds, Leeds, UK, [11]Applied Physics Laboratory, University of Washington, Seattle, WA, USA, [12]Atlantic Oceanographic and Meteorological Laboratory, National Oceanic and Atmospheric Administration, Miami, FL, USA, [13]Department of Oceanography, University of Hawai'i at Mānoa, Honolulu, HI, USA, [14]Department of Oceanography, Dalhousie University, Halifax, NS, Canada

Abstract Air-sea gas exchange regulates the exchange of climatically important gases between the ocean and the atmosphere, shaping both climate and ocean biogeochemistry. Bubbles beneath the sea surface enhance this exchange by introducing an additional transfer pathway in parallel to the interfacial transfer route. Although the role of bubbles in gas flux has been debated since the 1980s, recent advances in laboratory experiments, field observations, and modeling have provided new insights. Bubble-mediated gas transfer differs from interfacial transfer in three key ways: (a) it shows strong nonlinearity with wind speed due to its link with wave breaking; (b) it depends on gas solubility because of the finite volume and short lifetime of bubbles; and (c) it shifts the equilibrium toward slight oversaturation through the overpressure of submerged bubbles. These characteristics make bubble-mediated gas transfer complicated to quantify, and existing observations and models indicate a wide range of bubble contributions to air-sea carbon dioxide and oxygen exchange. Three critical knowledge gaps are identified: (a) limited understanding of near-surface (0–1 m) bubble dynamics, including volume flux, size distribution, and evolution, which directly control the solubility and diffusivity dependence of bubble-mediated gas exchange; (b) the absence of consistent field constraints spanning the full range of gas solubilities; and (c) the lack of knowledge to scale laboratory results to oceanic conditions. Addressing these gaps will require integrated efforts combining near-surface bubble measurements and simulations, field observations of gas transfer across diverse solubilities using complementary techniques, and improved modeling frameworks.

Plain Language Summary Air-sea gas exchange is a key process linking the ocean and the atmosphere, influencing both Earth's climate and the health of ocean ecosystems. For instance, the ocean takes up about one-quarter of the carbon dioxide (CO_2) released by human activities through this exchange. While gases can transfer directly across the sea surface, breaking waves create bubbles that offer an additional route for gas exchange. Bubble-mediated gas transfer is complex, as the limited volume and lifetime of bubbles make it dependent on gas solubility and driven by intricate bubble dynamics and near-surface water movement. Studies report a wide range of bubble contributions to air-sea CO_2 or oxygen exchange, spanning roughly an order of magnitude. In this review, we synthesize progress in understanding the role of bubbles in air-sea gas exchange, drawing on advances from theory, laboratory experiments, field observations, and modeling studies over recent decades. Building on this synthesis, we identify key knowledge gaps and outline priorities for future research.

1. Introduction

The air-sea exchange of poorly soluble gases (Table 1) such as carbon dioxide (CO_2), methane (CH_4), nitrous oxide (N_2O), oxygen (O_2), and dimethylsulfide (DMS) plays a crucial role in regulating Earth's climate and ocean ecosystems (Lee et al., 2023). The global ocean takes up approximately a quarter of the CO_2 emitted by human

Software: Yuanxu Dong
Supervision: Bernd Jähne, Christa A. Marandino
Validation: Yuanxu Dong, Bernd Jähne, David K. Woolf, Kerstin E. Krall, Mingxi Yang, Helen Czerski, Junhong Liang, Ian M. Brooks, Craig L. McNeil, Rik Wanninkhof, Christa A. Marandino
Visualization: Yuanxu Dong, Bernd Jähne, David K. Woolf, Kerstin E. Krall, Mingxi Yang, Helen Czerski, Junhong Liang, Craig L. McNeil, Rik Wanninkhof, Christa A. Marandino
Writing – original draft: Yuanxu Dong
Writing – review & editing: Yuanxu Dong, Bernd Jähne, David K. Woolf, Kerstin E. Krall, Mingxi Yang, Helen Czerski, Junhong Liang, Ian M. Brooks, Craig L. McNeil, Rik Wanninkhof, David T. Ho, Dariia Atamanchuk, Christa A. Marandino

Table 1
General Research Fields and Selected References Related to Bubble-Mediated Gas Exchange

Key research fields	Example references
Bubble-mediated gas transfer velocities and bubble-induced supersaturation	References discussed in this review
Wave breaking, upper ocean and bubble dynamics, and whitecap coverage	Monahan and Mac Niocaill (1986); Deane and Stokes (2002); Sullivan and McWilliams (2010); Deike et al. (2016); Brumer, Zappa, Brooks, et al. (2017); Deike (2022); Czerski et al. (2022a, 2022b); Ruth et al. (2022); Callaghan et al. (2025)
Scaling bubble effects to the regional/global ocean	Atamanchuk et al. (2020); Reichl and Deike (2020); Sun et al. (2023); Zhou et al. (2023); Rustogi et al. (2025); Deike et al. (2025); Dong et al. (2025)

activities (Friedlingstein et al., 2025), partially alleviating global warming, but also leading to ocean acidification (Doney et al., 2009). Understanding air-sea gas exchange is essential for accurately assessing the global carbon budget, projecting future climate and the oceanic environment, and developing possible climate mitigation strategies like marine carbon dioxide removal (mCDR; e.g., Doney et al., 2024).

This review focuses on poorly soluble gases only, for which bubble-mediated transfer can be effective, whereas it is negligible for highly soluble gases (see Section 2). For poorly soluble gases, their air-sea exchange is primarily limited by the waterside diffusion layer (Liss & Slater, 1974) and facilitated by near-surface turbulence (Wanninkhof et al., 2009). Wind transfers momentum to the sea surface, generating a shear layer and surface turbulence that drive gas exchange across the air-sea interface (i.e., interfacial transfer; Figure 1). At the same time, wind stress generates waves, and field observations indicate that waves may start breaking at U_{10} (10-m height wind speed above the mean sea level) of 4–5 m s^{-1} (e.g., Callaghan et al., 2008). Wave breaking produces bubbles that entrain air into the water, providing an additional pathway for gas exchange (i.e., bubble-mediated gas exchange; Figure 1). The air-sea gas exchange flux can be expressed as:

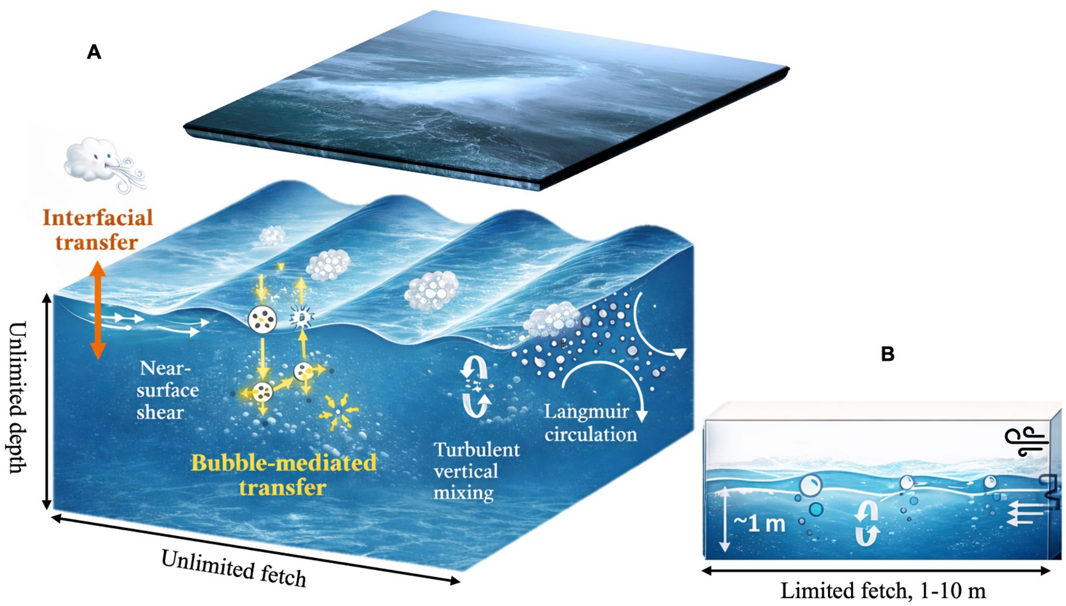

Figure 1. A conceptual schematic of air-water gas exchange in the open ocean (a) and wave tank (b). The air-sea gas transfer comprises interfacial transfer (orange arrow) and bubble-mediated transfer (yellow arrows, invasion scenario). Various physical processes, including wind, waves, wave breaking, near-surface shear, Langmuir circulation, and turbulent vertical mixing, govern gas exchange (Woolf, 1997). Coastal and laboratory experiments should be interpreted according to their ability to mimic physical processes controlling air-sea gas exchange in the open ocean. The overlaying photo was taken during a research cruise under intense wave-breaking conditions.

$$F = k(C_w - HC_a) \quad (1)$$

where k (m s^{-1}) is the total gas transfer velocity, including both the interfacial transfer (k_i) and the bubble-mediated transfer (k_b) components. H is the dimensionless Henry's law solubility (ratio of gas concentration in water to that in air at equilibrium), equivalent to the non-dimensional Ostwald solubility (α) commonly used in air-water gas exchange studies (Sander, 2023). It can be converted to the dimensional aqueous-phase solubility K_0 (mol m^{-3} Pa^{-1}) in large-scale models as $K_0 = H\,(R\,T_w)^{-1}$ (Wanninkhof et al., 2009), where R (m^3 Pa K^{-1} mol^{-1}) is the ideal gas constant and T_w (K) is the water temperature. C_w and C_a are gas concentrations (e.g., in mol m^{-3}) in the surface ocean and lower atmosphere, respectively. For air-sea CO_2 flux, $(C_w - HC_a)$ is often expressed as $K_0 \Delta f CO_2$, where $\Delta f CO_2 = f CO_{2w} - f CO_{2a}$ is the CO_2 fugacity (μatm) difference between the surface seawater and the lower atmosphere. Note that Equation 1 does not explicitly include bubble-induced asymmetric transfer flux (see Section 2.1).

The interfacial and bubble-mediated transfer processes exhibit substantially different characteristics.

First, gas exchange through the unbroken air-sea interface is primarily driven by the wind-induced shear turbulence. The boundary layer theory that links turbulence to wind stress, combined with eddy-renewal theory, predicts that the interfacial transfer velocity (k_i) scales with friction velocity (u_*, a proxy for surface shear), yielding a near-linear dependence of k_i on U_{10} (Deacon, 1977; Fairall et al., 2011; Jähne et al., 1987). Differently, the bubble-mediated gas exchange is directly linked to wave breaking, a wave energy dissipation process, which in turn has a strongly nonlinear relationship with wind speed (Goddijn-Murphy et al., 2016; Monahan & O'Muircheartaigh, 1986; Terray et al., 1996).

Second, interfacial transfer of poorly soluble gases is limited by molecular diffusion through the waterside boundary layer, making k_i depend on molecular diffusivity (D) or Schmidt number (Sc, defined as the ratio of water's kinematic viscosity to D). For comparison across gases and temperatures, k_i is often normalized to a reference Sc (e.g., 660, equal to the Sc of CO_2 at 20°C) using $k_{i660} = k_i(660/Sc)^{-n}$. In contrast, bubble-mediated gas transfer velocity (k_b) depends not only on diffusion but also on gas solubility. For high-solubility gases, equilibration between the bubble and the surrounding seawater occurs rapidly due to limited bubble volume, after which exchange effectively ceases for the remainder of the bubble lifetime. This limits the total effective exchange time and results in a low transfer velocity. This process can be likened to a sprint versus a marathon: highly soluble gases equilibrate quickly, like a sprinter's brief burst, exhausting the bubble's exchange capacity, whereas poorly soluble gases equilibrate more slowly, like a marathon runner, remaining out of equilibrium longer and sustaining transfer over an extended period. Consequently, despite slower instantaneous flux, poorly soluble gases achieve greater integrated bubble-mediated transfer.

Third, interfacial transfer occurs at sea level pressure, yielding 100% saturation under complete equilibrium. Entrained bubbles, however, experience hydrostatic pressure and Laplace pressure (forced by surface tension), leading to internal overpressure and complete dissolution in very small bubbles. This favors gas invasion over evasion, and shifts the equilibrium to slight oversaturation.

Although interfacial and bubble-mediated transfer have these distinct properties, Equation 1 does not explicitly separate them. While this formulation is commonly applied in global ocean gas flux estimates, it may introduce significant uncertainties, particularly under high-wind conditions where bubble-mediated exchange becomes significant. The potential role of bubbles in air-sea gas exchange was first recognized in the 1960s (Bolin, 1960; Kanwisher, 1963). Subsequently, theoretical and modeling studies (Jähne et al., 1984; Keeling, 1993; Memery & Merlivat, 1985; Woolf, 1993, 1997; Woolf & Thorpe, 1991) as well as laboratory experiments (Asher et al., 1996; Broecker & Siems, 1984; Krall et al., 2019; Rhee et al., 2007) identified the key properties of bubble-mediated transfer discussed above. Observations and simulations of wave breaking, bubble dynamics, and whitecap coverage (e.g., Deane & Stokes, 2002; Deike, 2022; Liang et al., 2013; Monahan & Mac Niocaill, 1986) have significantly improved our ability to model bubble-mediated gas exchange. Measurements of supersaturation for the least soluble gases, such as noble gases and N_2 (e.g., Farmer et al., 1993; Hamme et al., 2017; Stanley et al., 2009; Stanley et al., 2022; Wallace & Wirick, 1992), along with eddy covariance (EC) observations of air-sea CO_2 and DMS transfer velocities (e.g., Bell et al., 2017; Blomquist et al., 2017; Zavarsky et al., 2018), provide valuable constraints for the quantification of bubble-mediated transfer velocities (Deike & Melville, 2018; Fairall et al., 2022) and bubble-induced asymmetric transfer (Deike et al., 2025; Dong et al., 2025).

Despite substantial progress, quantifying bubble-mediated transfer remains challenging. Table 1 outlines the main research domains in this field. In this work, we focus on bubble-mediated gas transfer velocities and bubble-induced supersaturation. Related topics, such as bubble and upper-layer water dynamics, are equally important, but are beyond our scope (please refer to the relevant literature listed in Table 1). For readers interested in the broader topic of air-sea gas exchange, several classic (Garbe et al., 2014; Wanninkhof et al., 2009) and recent reviews (Bange et al., 2024; Stanley & Bell, 2025) provide comprehensive overviews. Here, we begin with the theoretical frameworks of bubble-mediated gas exchange, followed by laboratory experiments, field observations, and modeling efforts. The discussion concludes with a synthesis, highlighting unresolved questions and priorities for future research. Although the mechanisms discussed apply broadly to all poorly soluble gases, we place special focus on CO_2 and O_2 due to their climate and biology relevance and the ongoing debate about the role of bubbles in their exchange.

2. Theory

2.1. Bubble-Mediated Gas Exchange Frameworks

The traditional bulk formulation (Equation 1) does not explicitly account for the contribution of bubbles to air-sea gas exchange. To address this limitation, two theoretical frameworks have been independently proposed and are widely used to explicitly represent bubble-mediated gas exchange: the Woolf (1993) framework and the Keeling (1993) framework.

Woolf (1993) framework. In the Woolf framework, the total gas transfer velocity is decomposed into an interfacial component, k_i, and a bubble-mediated component, k_b. The effect of bubble compression is totally attributed to an overpressure factor, δ, or a supersaturation factor, Δ_s, in the revised bulk formulation. The bubble-mediated transfer flux component (F_b) and interfacial transfer flux component (F_i) are written as

$$F_b = k_b [C_w - (1 + \delta) H C_a] \quad (2)$$

$$F_i = k_i (C_w - H C_a) \quad (3)$$

and the total air-sea gas flux is

$$F = (k_i + k_b) [C_w - (1 + \Delta_s) H C_a] \quad (4)$$

where

$$\Delta_s = \delta k_b / (k_i + k_b) \quad (5)$$

Here, δ represents the fractional overpressure experienced by gases inside bubbles, while Δ_s represents supersaturation that would be observed under equilibrium conditions with no net air-sea exchange (Woolf, 1997). Δ_s is always smaller than δ, because Δ_s reflects the combined effects of bubble-mediated and interfacial transfer as bubble-induced supersaturation is partially relaxed by interfacial exchange (Leighton et al., 2018). For clarity, we refer to δ as the overpressure factor and Δ_s as the supersaturation factor.

In this framework, all bubble-related transfer velocity is attributed to k_b, while the compression effect of bubbles (including both partially dissolving large bubbles and fully dissolving small bubbles) is subsumed into δ (or Δ_s). As a result, k_b is independent of gas saturation state and is identical for gas invasion and evasion.

Keeling (1993) framework. Keeling (1993) proposed an alternative framework in which both the bubble-associated exchange rate and the bubble-induced supersaturation are embedded in saturation-dependent transfer velocities. Separate bubble-mediated transfer velocities are defined for pure invasion scenario (i.e., $C_w = 0$) and pure evasion (i.e., $C_a = 0$), k_b^{in} and k_b^{out}, respectively. The bubble-mediated transfer flux is then

$$F_b = k_b^{out} C_w - k_b^{in} H C_a \quad (6)$$

and the total gas transfer flux becomes

$$F = \left(k_i + k_b^{\mathrm{out}}\right)\left(C_w - HC_a\right) + \left(k_b^{\mathrm{out}} - k_b^{\mathrm{in}}\right)HC_a \tag{7}$$

The corresponding supersaturation factor can be expressed as

$$\Delta_s = \left(k_b^{\mathrm{in}} - k_b^{\mathrm{out}}\right)/\left(k_i + k_b^{\mathrm{out}}\right) \tag{8}$$

Algebraically, the Woolf and Keeling frameworks are equivalent. By assigning the pure evasion (i.e., $C_a = 0$) and pure invasion scenarios (i.e., $C_w = 0$), and combining Equations 2 and 6, the following relations are obtained

$$k_b^{\mathrm{out}} = k_b \tag{9}$$

$$k_b^{\mathrm{in}} = (1+\delta)k_b \tag{10}$$

It is worth noting that the definition of invasion (evasion) transfer velocity represents the pure invasive (evasive) process, instead of the net invasion (evasion). A detailed comparison and translation between the two frameworks, along with links to bubble dynamical models, is provided in Table A1 in the Appendix.

Despite their mathematical equivalence, the two frameworks differ in physical interpretation. Bubble compression increases gas concentrations within bubbles, thereby favoring gas exchange to the invasive direction and shifting the equilibrium toward supersaturation. However, compression does not alter turbulence or molecular diffusivity and therefore should not affect the transfer velocity itself. From this perspective, the Woolf framework provides a more physically transparent separation between exchange kinetics (k_b) and thermodynamic effects through δ or Δ_s on gas concentration difference. Nevertheless, studies interpreted using the Keeling framework have significantly advanced our understanding of bubble-induced supersaturation (e.g., Deike et al., 2025). Accordingly, throughout the remainder of this review, we primarily adopt the Woolf framework and explicitly indicate where the Keeling framework is used in the studies discussed.

2.2. Linking Bubble-Mediated Gas Transfer With Bubble Dynamics

Woolf (1993) presents a detailed derivation of gas exchange processes for a single bubble and its integration over the entire bubble plume. Here, we highlight only the key parameters relevant for understanding the properties of bubble-mediated gas exchange. For a specific bubble with a radius of r and a single bubble transfer velocity of k_{sb}. Through exchange with the surrounding seawater, the gas within the bubble will reach equilibrium exponentially, and the equilibrium (e-folding) time (τ_e) is given as

$$\tau_e = r/(3k_{sb}H) \tag{11}$$

This suggests that more soluble gases equilibrate more rapidly. But for gases with very low solubility, equilibrium may not be reached within the bubble lifetime (τ_b, the time that the bubble stays in the water column). Integrating the bubble-mediated exchange for the whole bubble lifetime and considering the entire bubble flux, the total bubble-mediated gas transfer velocity can be expressed as:

$$k_b = \int Q(r)\left(1 - e^{-\tau_b/\tau_e}\right)4\pi r^3/(3H)\,dr \tag{12}$$

where $Q(r)$ is the bubble size distribution, which represents the number of bubbles with different radii entrained per unit sea-surface area per unit time ($\mathrm{m^{-2}\ s^{-1}}$).

Two limiting regimes emerge naturally. If $\tau_b/\tau_e \ll 1$, such that equilibration is slow relative to bubble lifetime,

$$k_b = \int Q(r)\tau_b 4\pi r^2 k_{sb}dr \approx S_b\tau_b k_{sb}, \qquad \tau_b/\tau_e \ll 1 \tag{13}$$

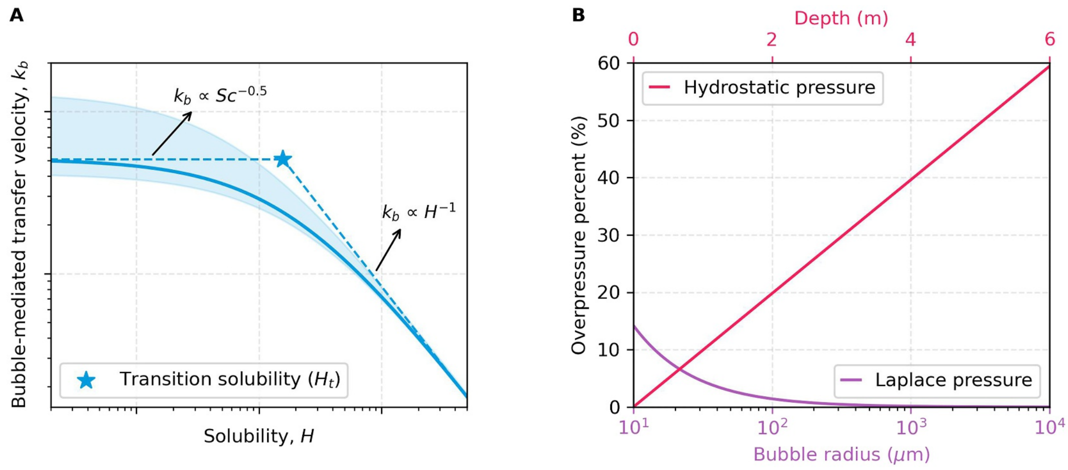

Figure 2. Bubble-mediated gas transfer properties. (a) Schematic of the solubility dependence of bubble-mediated gas transfer velocity (k_b, blue curve), with the shaded areas capturing variations in the Schmidt number (Sc). The star represents the transition solubility (H_t), which is the approximate point to separate the H dependence and the Sc dependence (made from Woolf, 1997; Krall et al., 2019). (b) Overpressure of the gas in the bubble due to the water's hydrostatic pressure versus depth (red) and due to the curved surface-induced Laplace pressure versus the bubble radius (purple).

where S_b (m^2 m^{-2} s^{-1}) is the total bubble surface area per unit sea-surface area per unit time. This approximation (i.e., $k_b \approx S_b \tau_b k_{sb}$) assumes that $\tau_b k_{sb}$ depends weakly on bubble radius, which is plausible because larger bubbles rise faster but also exhibit higher transfer velocities (Levich, 1962; Memery & Merlivat, 1985).

In contrast, if $\tau_b/\tau_e \gg 1$, equilibration is effectively instantaneous and

$$k_b = \int Q(r)\, 4\pi r^3/(3H)\, dr = V_b/H, \qquad \tau_b/\tau_e \gg 1 \tag{14}$$

where V_b (m^3 m^{-2} s^{-1}) is the total bubble volume flux per unit sea-surface area per unit time, which is also called the "flushing rate" (Woolf, 1997) or "air entrainment velocity" (Deike & Melville, 2018; Keeling, 1993).

It is worth noting that for gases of any solubility, bubble-mediated exchange becomes potentially significant only when the total bubble surface area approaches that of the sea surface (e.g., Vlahos & Monahan, 2009; Woolf, 2025). Equation 13 indicates that for the very low-solubility gases, k_b scales with the single-bubble transfer velocity (Figure 2a). Therefore, in this regime, bubble-mediated exchange mirrors interfacial exchange and is expected to exhibit Schmidt number dependence, and bubbles just provide additional surface (S_b) for gas exchange. Conversely, Equation 14 shows that exchange of high-solubility gases is controlled by the bubble volume flux and is inversely proportional to solubility (Figure 2a). The transition between these regimes occurs at a characteristic solubility (Figure 2a):

$$H_t = V_b/(S_b \tau_b k_{sb}) \tag{15}$$

where H_t represents the transition solubility that separates the k_b into approximately two regimes (i.e., the H dependence and the Sc dependence). Gases with solubility near H_t are expected to exhibit complex dependence on both H and Sc. H_t depends on the ratio of total bubble volume to total bubble surface area, which is governed by the bubble size distribution. For example, switching from seawater to freshwater shifts the bubble size distribution toward larger radii (Cartmill & Su, 1993), increasing the bubble volume-to-surface-area ratio and, consequently, increasing H_t. H_t is also influenced by bubble lifetime and the single-bubble transfer velocity. The former is controlled by the penetration depth and the rising speed, which depend on bubble size, while the latter depends on both bubble size and bubble surface cleanliness (i.e., "dirty" or "clean"). Taken together, H_t is primarily determined by the bubble size distribution, and secondly by the bubble penetration depth and behavior.

The bubble-induced supersaturation factor (Δ_s) cannot be expressed as compactly as k_b. From Equation 5, Δ_s depends on both the overpressure factor (δ) and the relative importance of bubble-mediated versus interfacial

Table 2
Gas Categories According to Their Dimensionless Solubilities (H)

Gas category	Poorly soluble gases: The least soluble	Poorly soluble gases: Moderately soluble	Poorly soluble gases: Soluble	Highly soluble gases
Controlled phase	Waterside			Airside
Solubility range	$H \leq 0.05$	$0.05 < H < 5$	$5 \leq H < 500$	$H \geq 500$
Example	SF_6, ^3He, N_2, O_2, CH_4	CO_2, N_2O	DMS	H_2O, methanol, acetone

transfer. The value of δ is controlled by bubble penetration depth (Figure 2b) and the vertical distribution of bubble sizes. Small bubbles generally penetrate deeper and persist longer, making them more influential for poorly soluble gases (e.g., O_2; Liang et al., 2013). Larger bubbles, by contrast, remain shallower, surface rapidly, and dominate the bubble volume flux, making them more important for soluble gases (e.g., CO_2; Keeling, 1993). Therefore, δ (and Δ_s) depend on gas solubility. In addition, Δ_s also depends on the relative contribution from bubbles to the total gas exchange (see Equation 5). At high wind speeds, bubbles may dominate the exchange (e.g., contributes >90% of the total gas exchange), making Δ_s approach δ. The bubble compression effect is primarily due to the hydrostatic pressure, while Laplace pressure also contributes to overpressure, but is insignificant except for tiny bubbles smaller than 50 μm (Figure 2b).

The theoretical frameworks summarized above provide a basis for interpreting bubble-mediated gas exchange properties. The following sections review observational and modeling studies that quantify k_b and Δ_s and evaluate how well they support the theoretical expectations.

For clarity in the following discussion, we group poorly soluble gases into three categories based on the gases' solubility: (a) the least soluble gases ($H \leq 0.05$), (b) moderately soluble gases ($0.05 < H < 5$), and (c) soluble gases ($5 \leq H < 500$). Table 2 summarizes this classification along with representative examples. All the poorly soluble gases discussed in this study, along with their solubilities and Schmidt numbers at 20°C in seawater, are listed in Table A2.

3. Laboratory Studies

Laboratory experiments are indispensable for advancing our understanding of air-water gas exchange, as their controlled conditions allow key variables to be isolated and manipulated with precision and repeatability. The features of bubble-mediated gas exchange have been extensively investigated in the laboratory (Tables A3–A6), providing valuable insights into underlying mechanisms. Because laboratory tanks differ in design and operating conditions, we organize the review by classifying experiments according to tank type (Figure 3).

Before proceeding, we note that most laboratory studies estimate gas transfer velocities using Equation 1 without explicitly accounting for the bubble-induced supersaturation factor (Δ_s). Consequently, the bubble compression effect is implicitly incorporated into the inferred transfer velocity, in a manner analogous to the Keeling (1993) framework (see Section 2).

3.1. Results From Linear Wind-Wave Tanks Under Normal Winds

Traditional linear wind-wave tanks (Figure 3a) have long been used in air-sea gas exchange studies (Table A3), with bubbles generated primarily through wind-driven wave breaking. Mechanically generated waves are often added to promote wave development and facilitate breaking.

Broecker and Siems (1984) conducted evasion gas transfer experiments in the Hamburg wind-wave tank using O_2 and CO_2. They observed that O_2 transfer velocities exceeded those of CO_2 at reference wind speeds above 10 m s^{-1}, with the divergence increasing with wind speed (Figure 4a). This result likely represents the first laboratory evidence that bubble-mediated gas exchange is solubility dependent and significant for O_2. In contrast, subsequent experiments in both the small and the large Marseille linear wave tanks struggled to generate sufficient wave breaking, and no significant bubble effects were observed (Jähne et al., 1984; Merlivat & Memery, 1983; Rhee et al., 2007) unless bubbles were artificially introduced (see Section 3.2). Observations indicate

10.1029/2025RG000903

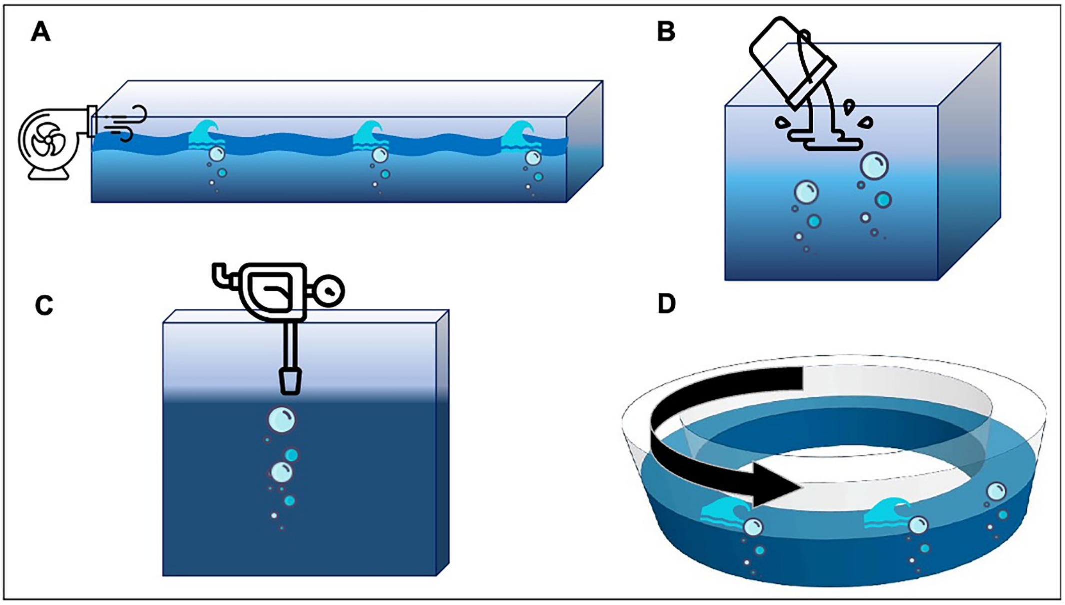

Figure 3. Experimental tank types used in bubble-mediated gas exchange studies. (a) Linear wind-wave tank with limited fetch and depth; (b) Whitecap simulation tank with tipping-bucket bubble generation; (c) Water box with plunging jet-generated bubbles; (d) Annular wind-wave tank with limited depth.

that substantially lower bubble concentrations are generated in the Marseille facility compared with the Hamburg tank (Jähne et al., 1984).

3.2. Results From Tanks With Introduced Bubbles

To overcome the difficulty of generating sufficient wave breaking in traditional wind-wave tanks, several studies have employed artificially introduced bubbles to highlight and isolate the bubble-mediated gas exchange (Table A4; Figures 3b and 3c).

Experiments in a large surf pool, where mechanically generated waves broke over a sloped floor, examined the exchange of the least soluble and moderately soluble gases (Asher et al., 1995; Wang et al., 1995; Wanninkhof et al., 1995). Transfer velocities were substantially larger for the least soluble gases, particularly under high whitecap coverage (Wanninkhof et al., 1995). McGillis et al. (1995) conducted complementary experiments in a small annular tank with artificial bubble injection and found enhanced O_2 transfer in seawater relative to freshwater, likely due to increased bubble surface area.

Subsequent experiments in a purpose-designed whitecap simulation tank using a tipping bucket (Figure 3b; Asher et al., 1996; Leifer et al., 1995) investigated exchange of gases spanning all poorly soluble subgroups (see Table 2). These studies demonstrated that bubbles are an efficient exchange pathway and revealed a clear solubility dependence of the transfer velocity. k_b was parameterized as a function of whitecap coverage and used for an empirical model development (see Section 5). Pronounced asymmetry between invasion and evasion was also observed. Total invasion transfer velocity exceeded evasion by ~50% for SF_6, ~5% for O_2, and was negligible for CO_2, corresponding to supersaturation factors of similar magnitude for each gas (Asher et al., 1996).

During the LUMINY gas exchange project, artificial aeration was used to generate bubbles in the large Marseille facility (Bowyer & Woolf, 2004; Rhee et al., 2007). Significant bubble effects were again observed for the least soluble gases (Rhee et al., 2007). Notably, high void fractions within bubble plumes were found to reduce bubble-mediated transfer, particularly for gases with low solubility and high diffusivity (Woolf et al., 2007). More recently, Mischler (2014) conducted experiments in a water box using jet-generated bubbles and more than 10 gases spanning the entire poorly soluble range (see Table 2 and Figure 4b). The results supported the theoretically predicted transition between Schmidt-number dependence for least soluble gases and solubility dependence for more soluble gases (Figure 2a). The experiment also showed that bubble-mediated transfer was stronger in the

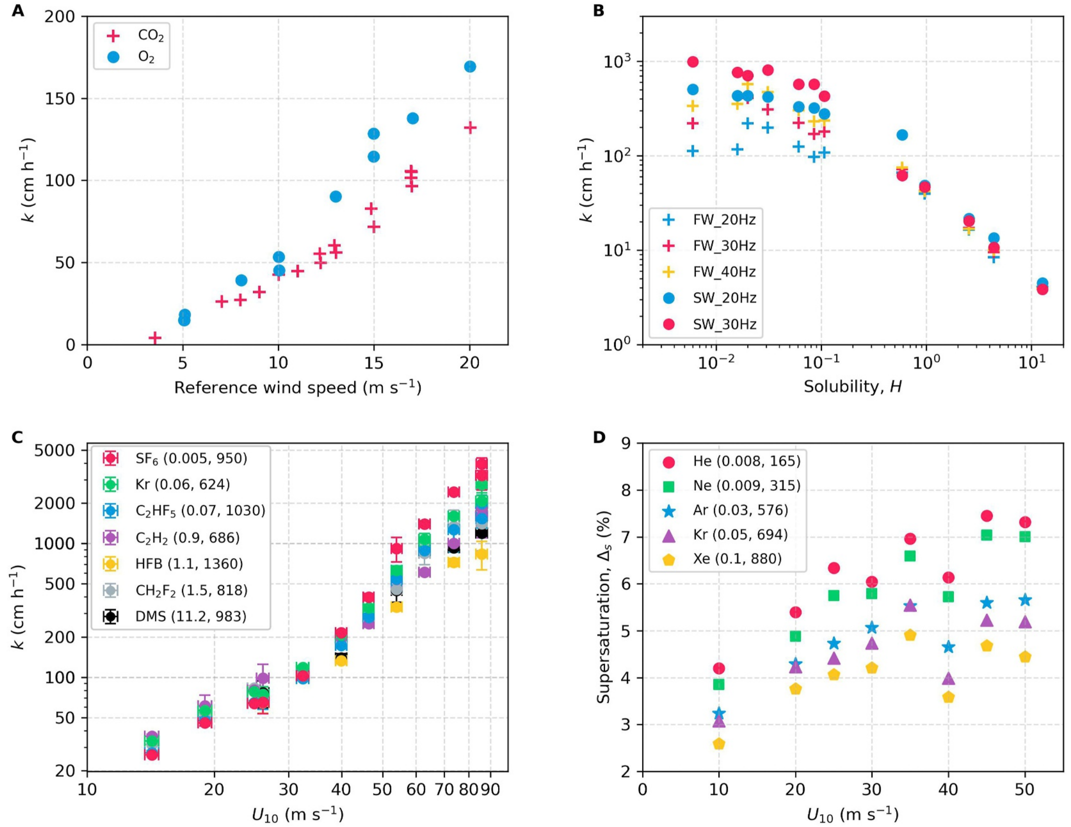

Figure 4. Gas transfer velocities and supersaturation fractions from laboratory studies. (a) Evasive transfer velocities of CO_2 (red pluses) and O_2 (blue dots) in the Hamburg linear wind-wave tank with freshwater (Broecker & Siems, 1984). (b) Evasive transfer velocities versus gas solubility in a water box with jet-generated bubbles at varying kinetic energies (Mischler, 2014). Different colors indicate varying plunging jet strengths, denoted by the driving frequency of the water pump. Both freshwater (FW, pluses) and artificial seawater (SW, 17.5‰, dots) were tested. (c) Evasive transfer velocities for gases of varying solubilities under hurricane conditions with seawater in the Miami SUSTAIN facility (Krall et al., 2019). Colors denote different gases; solubilities and Schmidt numbers are indicated in the legend. Error bars show ±1 standard deviation. (d) Supersaturation (Δ_s) (expressed in percentage) of noble gases observed in the Miami SUSTAIN facility with seawater under varying wind speeds (Stanley et al., 2022). The data shown here are averages from experiments with monochromatic and JONSWAP waves at 26°C. Solubilities and Schmidt numbers at 20°C seawater are shown for reference in the legend.

saltwater than in freshwater (Figure 4b), with transition solubilities shifting from ~0.06 in saltwater to ~0.23 in freshwater (Mischler, 2014).

3.3. Results From Annular Wind-Wave Tanks

Limited wave breaking in traditional linear wind-wave tanks arises not only from restricted wind forcing, but also from limited fetch and depth. Annular tanks, while still depth-limited, are not fetch-limited and therefore likely offer greater potential to simulate wind-driven wave breaking and bubble generation (Table A5).

McGillis et al. (1995) conducted gas exchange experiments in a small annular wave tank. They used both introduced bubbles (see Section 3.2) and wind-driven wave breaking, and in the latter configuration, invasive O_2 transfer velocities slightly exceeded evasion. The limited spatial scale of the tank restricts the representation of natural breaking-wave dynamics. Experiments conducted in the larger annular wind-wave tank at Heidelberg increased the scope of experimentation (Mesarchaki et al., 2015). Bubble concentrations observed in the large annular wave tank are approximately an order of magnitude higher than those measured in linear tanks at comparable wind speeds (Flothow, 2017).

3.4. Results From Linear Wind-Wave Tanks Under Hurricane Conditions

Advances in laboratory facilities have enabled high-speed linear wind-wave tanks capable of generating intense wave breaking and substantial bubble entrainment under hurricane-force winds (Table A6).

Three bubble-mediated gas exchange experiments have been conducted in the Kyoto high-speed wind-wave tank. The first, reported by Iwano (2013), observed a sharp increase in CO_2 evasion transfer velocity above ∼34 m s^{-1}, a feature that was also evident in two subsequent experiments. Using the same facility, Krall and Jähne (2014) examined two gases with different solubilities (HFB with H ∼1 and DFB with H ∼3) and found no significant difference below ∼40 m s^{-1}. However, at higher winds, the less soluble gas (HFB) exhibited transfer velocities up to ∼40% larger. Since only two gases were studied, the role of bubbles was not firmly concluded by the authors. Krall et al. (2019) extended these experiments to a broader range of poorly soluble gases (spanning solubilities from 0.005 to 150, Table A6) and to both freshwater and artificial seawater (filtered tap water with added traces of 1-Butanole which mimics the bubble distribution of salt water) in the Kyoto facility. In freshwater, transfer velocities showed little dependence on solubility, indicating an insignificant bubble contribution across all gases tested. In artificial seawater, transfer velocities for the least soluble gases were substantially larger, indicating significant bubble contributions. For gases with solubilities comparable to CO_2, bubble contributions remained below ∼10% even at equivalent 10-m wind speeds up to 68 m s^{-1}. The inferred transition solubility (∼0.4 in freshwater and ∼0.03 in artificial seawater) is broadly consistent with Mischler (2014) despite the very different experimental facilities.

Related experiments in the Miami SUSTAIN wind-wave tank further explored bubble-mediated gas exchange under hurricane conditions. Krall et al. (2019) found bubble-mediated transfer in seawater significant only for the least soluble gases at wind speeds above 33 m s^{-1} (Figure 4c), with a transition solubility comparable to that observed in the Kyoto facility for the artificial seawater. Stanley et al. (2022) imposed mechanical wave fields (monochromatic or JONSWAP) beneath the wind forcing and observed substantial bubble-induced supersaturation for all observed noble gases (spanning solubilities from ∼0.008 to 0.1) for wind speeds as low as 10 m s^{-1} (Figure 4d). The observed supersaturation increased with wind speed to ∼35 m s^{-1}, and then leveled off. This is consistent with theoretical predictions that supersaturation strengthens as the bubble contribution increases and approaches equilibrium once bubble-mediated transfer dominates the total exchange.

The results from Krall et al. (2019) and Stanley et al. (2022) are not directly comparable due to differing experimental configurations. In Stanley et al. (2022), the imposed mechanical wave field enhanced wave breaking and bubble effects relative to the purely wind-driven conditions in Krall et al. (2019). Moreover, Krall et al. (2019) conducted pure evasion experiments, whereas Stanley et al. (2022) examined invasion-dominated conditions, under which bubble-induced asymmetry may have enhanced exchange fluxes. This further highlights the sensitivity of bubble-mediated transfer quantification to experimental setup. Data from both high-speed wind-wave tanks have since been used to constrain bubble-mediated gas exchange models (see Section 5).

3.5. Uncertainties of the Laboratory Experiments

Laboratory studies have provided invaluable insights into bubble-mediated gas exchange, while also posing challenges in extrapolating results to natural conditions. Bubble-mediated transfer depends on bubble properties and associated dynamics such as wave breaking, bubble entrainment, initial bubble size distribution, penetration depth, and bubble plume evolution (Deike, 2022). Artificially introduced bubbles experience dynamics that differ fundamentally from those produced by wind-driven wave breaking in the ocean. While wind-wave tanks can generate wind-driven wave breaking, linear tanks are limited by fetch and depth, and annular tanks, though fetch-unlimited, remain depth-limited. As a result, open-ocean wave development, breaking, and bubble entrainment may not be fully reproduced in the tank. Upper-ocean dynamics, such as Langmuir circulation, strongly influence the formation of deep bubble plumes (depth >1 m; Thorpe, 2004; Liang et al., 2013). These processes are difficult to fully reproduce in laboratory tanks due to limitations such as the depth, yet they might be important for enhancing the supersaturation of the least soluble gases (Farmer et al., 1993; Stanley et al., 2009; Wallace & Wirick, 1992).

Moreover, natural air-sea gas exchange involves both invasion and evasion for many gases, such as CO_2, O_2, N_2, CH_4, N_2O, and noble gases, whereas DMS and SF_6/^{3}He during the dual-tracer experiments are purely evasive. Laboratory studies often infer transfer velocities using the Keeling (1993) framework, attributing bubble-induced asymmetry to k. Consequently, the derived k can differ between invasion and evasion, particularly near equilibrium. Finally, scaling laboratory hurricane experiments to the field remains challenging. In typical ocean environments (U_{10} of 0–20 m s^{-1}), transfer velocities, such as for CO_2, rarely exceed 100 cm hr^{-1} (see Section 4), whereas laboratory hurricane simulations report k values above 1,000 cm hr^{-1} (Krall et al., 2019), indicating that additional mechanisms such as spray-mediated exchange may become important and should be accounted (Woolf, 2025). Moreover, drag coefficient behavior at wind speeds above 40 m s^{-1} differs between laboratory (leveling off; Takagaki et al., 2012) and field observations (reduction; Powell et al., 2003), implying differences in momentum transfer that may also affect gas exchange scaling.

4. Field Observations

Field observations are essential for testing theoretical predictions, assessing laboratory results, and evaluating and constraining gas exchange models under natural conditions. In the field, strong evidence for bubble-mediated gas exchange in the least soluble gas regime comes from gas supersaturation observations, while for more soluble gases it is primarily inferred from EC air-sea CO_2 and DMS flux measurements.

4.1. Gas Supersaturation Measurements

The earliest evidence of bubble-mediated gas exchange likely comes from observations of persistent supersaturation of noble gases (i.e., He, Ne, Ar, Kr, Xe) in the ocean (e.g., Craig & Weiss, 1971). Because noble gases are inert and unaffected by biological processes, their supersaturation in surface waters provides a direct physical signature of bubble injection (e.g., Spitzer & Jenkins, 1989). The solubilities of noble gases span approximately an order of magnitude (~0.01–0.1), while their diffusivities vary by a factor of about five (Stanley et al., 2006). These properties allow differences in noble gas saturation states to be used to quantitatively infer bubble-mediated gas exchange (see Equation 8). Studies have consistently demonstrated that bubbles play a significant role in the exchange of these noble gases with very low solubilities (Hamme & Emerson, 2002, 2006; Hamme et al., 2017; Nicholson et al., 2011; Stanley et al., 2009).

Most noble gas-based analyses adopt the framework of Keeling (1993), which attributes the bubble-induced supersaturation to the transfer velocity and partitions it into contributions from partially dissolving large bubbles and fully dissolving small bubbles. This distinction is particularly important because, for the moderately soluble gases such as CO_2, large bubbles dominate bubble-mediated gas exchange, and the contribution of the fully dissolving bubbles is negligible. However, the relative contributions of these two bubble components inferred from field observations vary substantially among studies. Using timeseries of Ne, Ar, and N_2, Hamme and Emerson (2006) inferred an approximately equal contribution from partially dissolving and fully dissolving bubbles. In contrast, Stanley et al. (2009), who expanded the solubility range by additionally including observations of Kr and Xe, concluded that fully dissolving small bubbles accounted for more than 95% of the bubble-mediated flux. Extending these analyses using data from broader regions with stronger winds, Nicholson et al. (2011) inferred intermediate contributions from injected bubbles, falling between the results of Hamme and Emerson (2006) and Stanley et al. (2009). These differing estimates likely arise mainly from methodological differences, but some variability may also reflect different bubble size distribution under changing wind, wave, and upper-ocean conditions.

An alternative approach infers bubble effects from temporal changes in dissolved gas inventories (e.g., O_2, N_2, and noble gases) observed by high-resolution autonomous platforms (e.g., Craig & Hayward, 1987; Farmer et al., 1993; Wallace & Wirick, 1992). In this framework, the bubble contribution is estimated as the residual between observed inventory changes and those predicted by gas exchange parameterizations that neglect bubbles (e.g., Emerson & Bushinsky, 2016; Yang et al., 2017). Using O_2 and N_2 observations based on buoy and float collected during hurricane conditions, McNeil and D'Asaro (2007) and D'Asaro and McNeil (2008) found that gas exchange under the hurricane wind is dominated by bubble processes. They proposed a hurricane-specific gas exchange parameterization, which was later shown to be less applicable under lower wind conditions (Vagle et al., 2010). Notably, the O_2 transfer velocities estimated from hurricane-condition laboratory experiments (Krall et al., 2019) agree reasonably well with this field data-constrained model. Evidence of bubble-enhanced gas exchange under non-hurricane environments has also been reported. Koelling et al. (2017) and Atamanchuk et al. (2020) observed O_2 uptake in the central Labrador Sea that substantially exceeded estimates based on bubble-free parameterizations. Consistent results were also obtained from high-resolution N_2 observations

(Emerson & Bushinsky, 2016; Emerson et al., 2019) and from high-precision noble gas measurements (Seltzer et al., 2023), where accounting for bubble effects markedly improved agreement between modeled and observed gas inventories. While this inventory-based approach captures the integrated impact of bubbles, it does not directly constrain bubble-mediated transfer velocities. Moreover, the inferred bubble contribution remains sensitive to assumptions about background gas exchange and saturation state, leading to variability across gases and regions (Atamanchuk et al., 2020; Emerson et al., 2019; Ulses et al., 2021).

4.2. Eddy Covariance Observations

Strong field evidence for bubble-mediated exchange of the moderately soluble and soluble gases comes from EC air-sea CO_2 and DMS flux observations. The EC technique directly measures air-sea fluxes, from which gas transfer velocities are derived using both the EC flux and the air-sea concentration difference (Equation 2). Following the Woolf (1993) framework, the bubble compression effect is attributed to the supersaturation term (Δ_s), and the derived gas transfer velocity is free from the saturation state. For the soluble DMS, Δ_s is expected to be negligible, because bubble contributions are minimal and DMS exchange is almost exclusively evasive. In contrast, air-sea CO_2 exchange is naturally bidirectional, and therefore we adopt a nonzero Δ_s for CO_2 constrained by combined bubble observations, numerical modeling, and field data (Dong et al., 2025). Although this estimate carries substantial uncertainty, its impact on the transfer velocity analysis below is expected to be small. Multiple studies suggest that Δ_s for CO_2 is less than 1% (Liang et al., 2013; Stanley et al., 2009; Zhang, 2012) and likely on the order of 0.3%–0.5% on average globally (Deike et al., 2025; Dong et al., 2025; Leighton et al., 2018). This corresponds to a reduction in ΔfCO_2 of only ∼1–2 μatm relative to an atmospheric fugacity of ∼400 μatm (i.e., 0.3%–0.5% * 400 μatm). Because only EC data with $|\Delta fCO_2| > 20$ μatm are used to derive the CO_2 transfer velocity to minimize random flux uncertainty, the resulting bubble-induced asymmetry contributes less than a 10% effect. After assigning the Δ_s to Equation 2, the total transfer velocities for DMS and CO_2 can be derived, respectively, based on their corresponding EC flux measurements.

Although DMS belongs to the poorly soluble gas category, its solubility is much higher than that of CO_2, and bubbles should have minimal impact on DMS exchange, meaning that the observed total DMS transfer velocity ($k_{\_DMS}$) is dominated by the interfacial transfer (i.e., $k_{\_DMS} \approx k_{i\_DMS}$). Figures 5a and 5b present k_{660_DMS} from EC measurements collected from 12 cruises (see Table A7 for details; Bell et al., 2015, 2017; Blomquist et al., 2017; Blomquist et al., 2006; Huebert et al., 2010; Huebert et al., 2004; Marandino et al., 2007; Marandino et al., 2009; Miller et al., 2010; Yang et al., 2009, 2011; Zavarsky et al., 2018). The data show a near-linear relationship with U_{10}, consistent with theoretical predictions of the interfacial transfer (e.g., Fairall et al., 2011). The scatter in hourly k_{660_DMS} values likely reflects measurement uncertainties (Blomquist et al., 2010) and additional influences beyond wind speed, such as surfactants and convection (Wanninkhof et al., 2009).

Early attempts using the EC technique to measure air-sea CO_2 flux were mostly unsuccessful due to unrealistically large flux magnitudes and noise (Edson et al., 2011; Else et al., 2011; Jacobs et al., 2002; Kondo & Tsukamoto, 2007; Lauvset et al., 2011; Prytherch et al., 2010), and only a few cruises show reasonable results (McGillis et al., 2001, 2004). In the late 2000s, this bias was traced to water-vapor cross-sensitivity in the infrared gas analyzers (Blomquist et al., 2014; Landwehr et al., 2014; Miller et al., 2010; Nilsson et al., 2018). Miller et al. (2010) resolved this issue by drying the sample air, enabling accurate and precise air-sea CO_2 flux measurements. Figures 5c and 5d present high-quality (i.e., dried), ship-based CO_2 flux data from 14 open-ocean cruises (Bell et al., 2017; Blomquist et al., 2017; Butterworth & Miller, 2016; Dong, Yang, Bakker, Kitidis, & Bell, 2021; Dong, Yang, Bakker, Liss, et al., 2021; Dong et al., 2024; Ford et al., 2024; Landwehr et al., 2018; Miller et al., 2010; Yang et al., 2021, 2022; Zavarsky et al., 2018), spanning the full range of wind speeds under non-hurricane conditions. The results show that $k_{\_CO2}$ increases nonlinearly (nearly quadratically) with U_{10}, and is substantially higher at strong winds compared with k_{660_DMS} (Figures 5b and 5d), likely suggesting significant bubble contributions to CO_2 transfer. Noting that if bubble-mediated transfer is important, $k_{\_CO2}$ may depend on both Schmidt number (for the interfacial component) and solubility (for the bubble-mediated component). However, because the temperature sensitivity of $Sc^{-0.5}$ closely matches that of H^{-1}, normalizing $k_{\_CO2}$ by Sc or H yields nearly identical results (Figure A1). Here, we adopt the Schmidt-number normalization to make it consistent with previous studies.

Simultaneous CO_2 and DMS measurements provide direct constraints for bubble-mediated CO_2 transfer. Data from four cruises with sufficient concurrent measurements of CO_2 and DMS (Bell et al., 2015, 2017; Blomquist

10.1029/2025RG000903

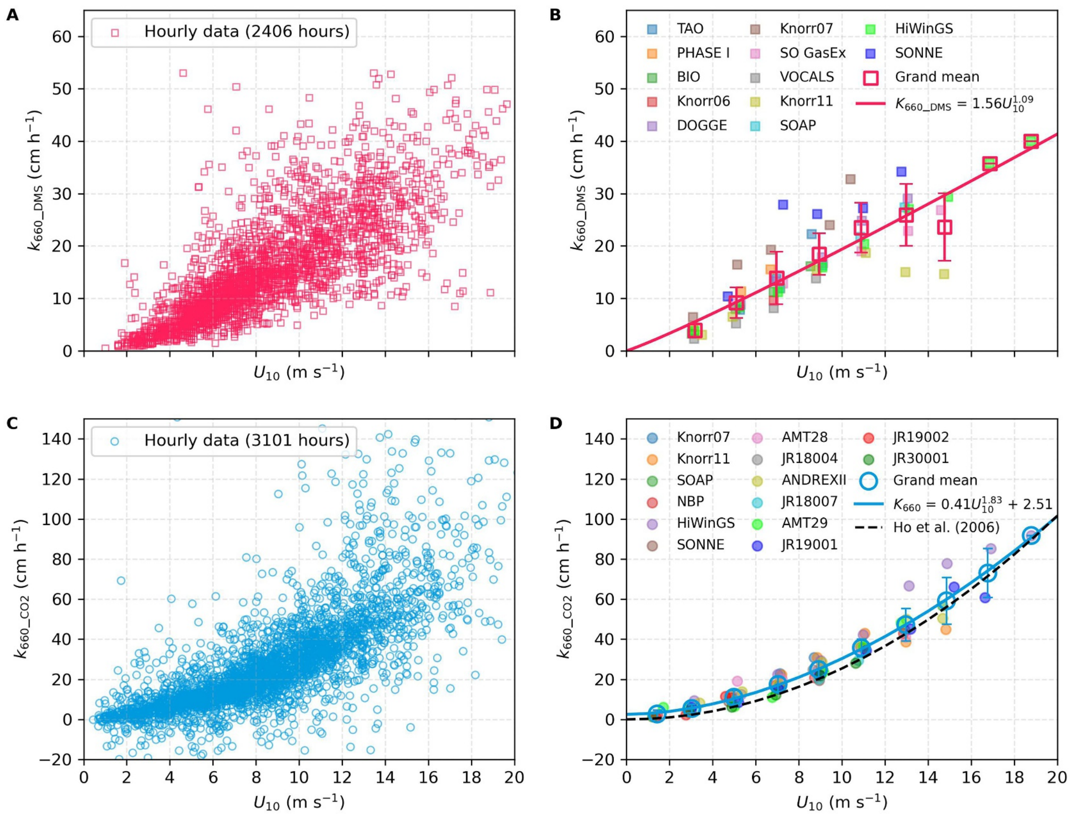

Figure 5. Gas transfer velocities derived from eddy covariance (EC) air-sea DMS and CO_2 flux observations. (a) DMS transfer velocity (k_{660_DMS}) derived from hourly DMS observations during 12 cruises (See Table A7). Note that the small airside resistance on DMS transfer has been corrected using the COAREG model (Fairall et al., 2022), and k_{660_DMS} present here is the waterside transfer velocity. (b) Bin averages of the hourly k_{660_DMS} by every 2 m s^{-1} wind speed (U_{10}) for each cruise. Red squares indicate the grand average of these bin-averaged points in each U_{10} bin, with error bars denoting 1 standard deviation. The red curve represents the fit according to the red squares ($R^2 = 0.98$), which shows a near-linear relationship with U_{10}. (c) CO_2 transfer velocity (k_{660_CO2}) derived from hourly EC CO_2 observations during 14 cruises (See Table A7). (d) Bin averages of the hourly k_{660_CO2} by every 2 m s^{-1} of U_{10} for each cruise. Blue circles indicate the grand average of these bin-averaged points in each U_{10} bin, with error bars denoting 1 standard deviation. The blue curve represents the fit according to the blue circles ($R^2 = 1$), which shows a strong non-linear relationship with U_{10}. For comparison, the k_{660}-U_{10} relationship based on a dual-tracer experiment is also plotted (Black line, Ho et al., 2006). Noting that the uncertainty in CO_2 measurements is significantly higher than DMS, which can result in k_{660_CO2} being less than zero. The numbers in panels (a) and (c) indicate the number of available data hours.

et al., 2017; Landwehr et al., 2018; Zavarsky et al., 2018) generally show that the $k_{\_CO2}$ exceeds $k_{\_DMS}$ under comparable conditions. The difference (i.e., $\Delta k = k_{\_CO2} - k_{\_DMS}$) generally increases with wind speed (Figures 6a and 6b). Notably, three cruises (two in the North Atlantic and one in the Southern Ocean) exhibit substantial Δk values, highlighting strong bubble contributions to CO_2 exchange. In contrast, the SONNE cruise in the tropical Indian Ocean shows $k_{\_CO2}$ values similar to other cruises, but significantly elevated $k_{\_DMS}$ at comparable wind speeds (blue squares, Figure 5b; Zavarsky et al., 2018), resulting in a negligible Δk. This anomaly may stem from vertical DMS gradients near the surface, as measurements there were taken at 5 m depth. Additionally, the SONNE cruise sampled fewer high wind speed data than the others. Worth noting that SONNE is the only cruise with a large fraction of net CO_2 evasion data points. However, because the bubble-induced asymmetry has been considered by including the Δ_s in Equation 2 when deriving $k_{\_CO2}$, the evasion data are unlikely to be the reason for the presented similar magnitudes of $k_{\_CO2}$ and $k_{\_DMS}$.

Parameterizations of $k_{\_CO2}$ and $k_{\_DMS}$ derived from the ensemble mean of these four cruises (Figure 6b) agree well with those based on the full data set (Figure 5), suggesting results from these four cruises can generally represent an average state of the diverse marine environments. Figures 6c and 6d show that Δk generally grows with U_{10}, becoming significant above 10 m s^{-1}. Because turbulence dissipation rate associated with wave

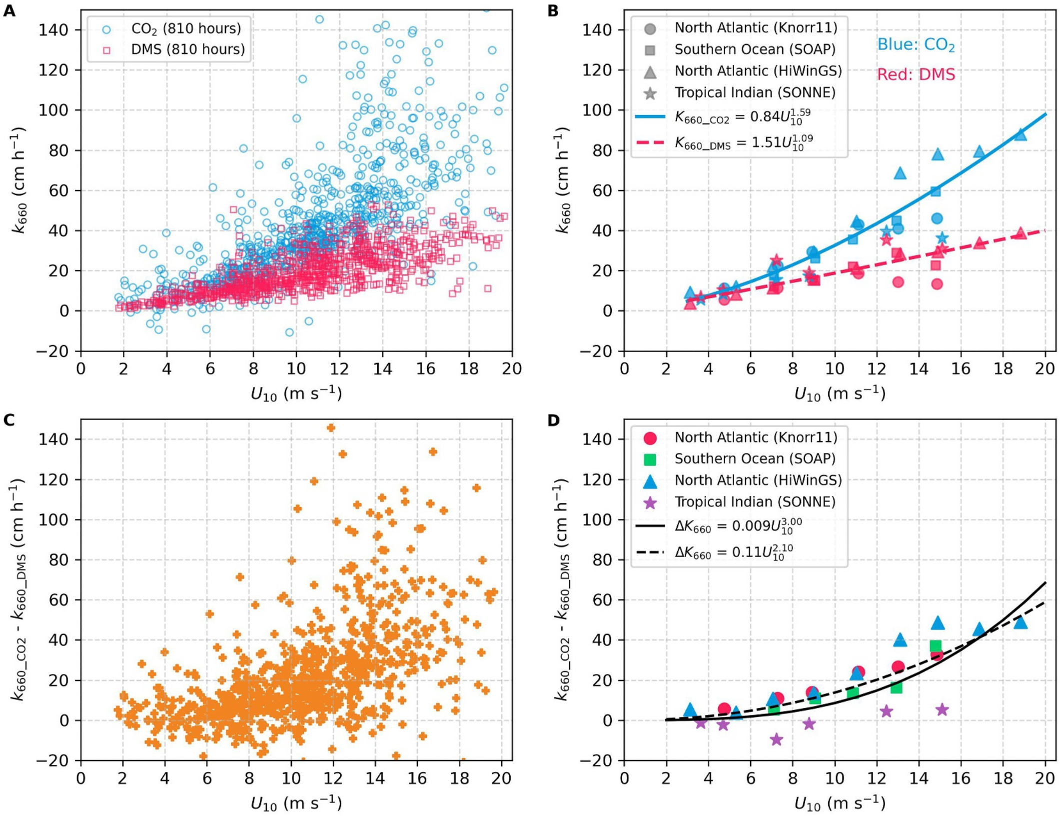

Figure 6. Simultaneous CO_2 and DMS transfer velocity observations in the open ocean. (a) Hourly CO_2 (k_{660_CO2}) and DMS (k_{660_DMS}) transfer velocity observations from four cruises (see Table A7). Note that there are a few points beyond 20 m s^{-1} wind speed for the HiWinGS cruise, which are not included here (see Blomquist et al., 2017). (b) 2 m s^{-1} bin averages (at least 3 data points in each bin) of the k_{660_CO2} (blue) and k_{660_DMS} (red) for different cruises with different markers corresponding to different cruises. The blue curve represents the fit based on the k_{660_CO2} bin averages (all the blue points, $R^2 = 0.98$), while the red line denotes the fit using the k_{660_DMS} bin averages (all the red points, $R^2 = 0.96$). (c) Difference between hourly k_{660_CO2} and k_{660_DMS} (Δk). (d) Bin averages of Δk for the four cruises. Solid-black and dashed-black lines correspond to the cubic fit ($R^2 = 0.92$) and the power-law fit ($R^2 = 0.98$) based on all the bin-averaged points, respectively. The numbers in panels indicate the number of available data hours.

breaking scales approximately with the cube of wind speed (Vassilicos, 2015), we fit the normalized Δk (i.e., Δk_{660}) with ${U_{10}}^3$, yielding the empirical parameterization ($R^2 = 0.92$):

$$\Delta k_{660} = 0.009 U_{10}^3 \tag{16}$$

A power-law fit was also tested ($\Delta k_{660} = 0.11 U_{10}^{2.10}$), which yields a higher R^2 (0.98). However, the data are scattered, and only a few points are available for U_{10} above 15 m s^{-1}, most of which were collected during the HiWinGS cruise. Therefore, although the power-law fit performs better statistically, the cubic fit is likely more physically consistent. Additional high-wind-speed data are needed to provide a more robust constraint on Δk_{660}. Interestingly, the coefficient 0.009 aligns well with the coefficient for the ${U_{10}}^3$ (=0.011) term used in the hybrid $k_{\_CO2}$ formulation of Wanninkhof et al. (2009), who linked CO_2 exchange to whitecap coverage, following the approach of Woolf (2005). Variability in Δk among cruises likely reflects differences in bubble dynamics, near-surface processes, and surfactant effects under differing sea states, suggesting that wind alone cannot fully describe Δk. Many studies have emphasized that k_{b_CO2} is strongly dependent on sea state (Brumer, Zappa, Blomquist, et al., 2017; Deike et al., 2025; Deike & Melville, 2018; Woolf, 2005; Yang et al., 2024; Zhao et al., 2003; Zhou et al., 2023). Regression of all hourly Δk_{660} data against U_{10}, u_*, significant wave height (H_s), and $u_* H_s$ shows that $u_* H_s$ yields the highest R^2, with H_s alone giving the second-highest (Figure A2). This further indicates that Δk is closely tied to wave parameters, and that wind speed alone cannot fully characterize the difference in the gas transfer velocity between CO_2 and DMS. Fitting the hourly Δk_{660} against ${u_*}^a {H_s}^b$ yields:

$$\Delta k_{660} = 9.7 u_{*}^{0.5} H_s^{1.1} \quad (17)$$

For a fully developed sea with infinite fetch, the significant wave height can be approximately parameterized as proportional to ${U_{10}}^2$ (Pierson & Moskowitz, 1964), and the friction velocity u_* as proportional to U_{10}. This implies that Equation 17 yields $\Delta k_{660} \propto {U_{10}}^{2.7}$, which does not differ significantly from the assumption underlying Equation 16. While Equation 17 captures sea-state-related variability, it is based on a limited range of conditions sampled during four cruises. In contrast, Equation 16 should be regarded as an approximate ensemble-mean parameterization that does not explicitly account for sea-state effects.

4.3. Uncertainties of the Field Observations

Field observations indicate that the supersaturation states of noble gases, as well as the temporal variability of N_2 and O_2, cannot be fully explained without invoking bubble-mediated gas exchange. Using the mass-balance approach, the bubble contribution to the gas exchange can be inferred. However, this method is sensitive to uncertainties in noble gas solubility estimates and their temperature dependence (Stanley et al., 2009), with more recent solubility measurements and parameterizations showing increased precision and greater solubilities by up to 2% (Jenkins et al., 2019). It also depends on the robustness of the budget analysis for other relevant processes (Atamanchuk et al., 2020). Furthermore, extrapolating bubble effects from the least soluble gases to more soluble gases requires accurate knowledge of the solubility dependence of bubble-mediated exchange. Both theoretical considerations (Section 2) and laboratory results (Section 3) suggest that this dependence may differ substantially between the least soluble and more soluble gases. Consequently, caution is warranted when scaling bubble effects inferred from noble gases to moderately soluble gases such as CO_2.

EC observations of air-sea CO_2 and DMS fluxes provide independent field-based evidence for the role of bubbles in moderately soluble and soluble gases. These measurements generally indicate that bubble-mediated exchange is negligible for DMS (Figures 5 and 6) but significant for CO_2. However, there is at least one cruise that did not show a significant difference between the observed CO_2 and DMS transfer velocities (Zavarsky et al., 2018). In addition, it remains unclear why EC-derived k_{660_CO2} are not substantially lower than k_{660} values obtained from dual-tracer ($^3He/SF_6$) experiments (Figure 5d), given that ^3He and SF_6 are far less soluble than CO_2 (Asher & Wanninkhof, 1998). A physical bubble model suggests that under the 'dense plume' assumption, where interstitial water gas content changes over a plume's lifetime (Woolf et al., 2007), the bubble contribution to CO_2 may be only slightly lower than that for $^3He/SF_6$ (Goddijn-Murphy et al., 2016). Nevertheless, additional observational evidence is needed to rigorously evaluate this hypothesis. It is also worth noting that the existing dual-tracer data set contains only a small number of measurements at wind speeds exceeding 12 m s^{-1}, limiting its ability to robustly constrain bubble-mediated exchange under high-wind conditions.

Finally, because bubble-mediated gas exchange is intrinsically linked to bubbles, direct observations of bubbles are essential for validating and complementing gas-based inferences. Bubble measurements also provide a critical bridge between laboratory experiments and field observations. However, such measurements are absent from most existing observational studies.

5. Models

As discussed above, bubble-mediated gas transfer is a complex process that arises from the coupled effects of gas exchange mechanisms and the bubble dynamics. Models of these processes comprise two core components: (a) representation of the solubility and Schmidt number dependence, which enables scaling across different gases; and (b) estimation of the bubble volume flux, which sets the magnitude of bubble-mediated gas exchange. A comprehensive model must therefore correctly describe the solubility and Schmidt number dependence and accurately quantify the magnitude of bubble volume flux. Over the past several decades, a range of models, spanning physically based and empirically based approaches, have been developed to describe bubble-mediated gas exchange (Table A8).

5.1. Bubble Dynamics

In the physical bubble models, bubble dynamics, including bubble generation, penetration, and evolution, as well as the bubble size distribution, are simulated and coupled to gas exchange processes. Before reviewing the bubble

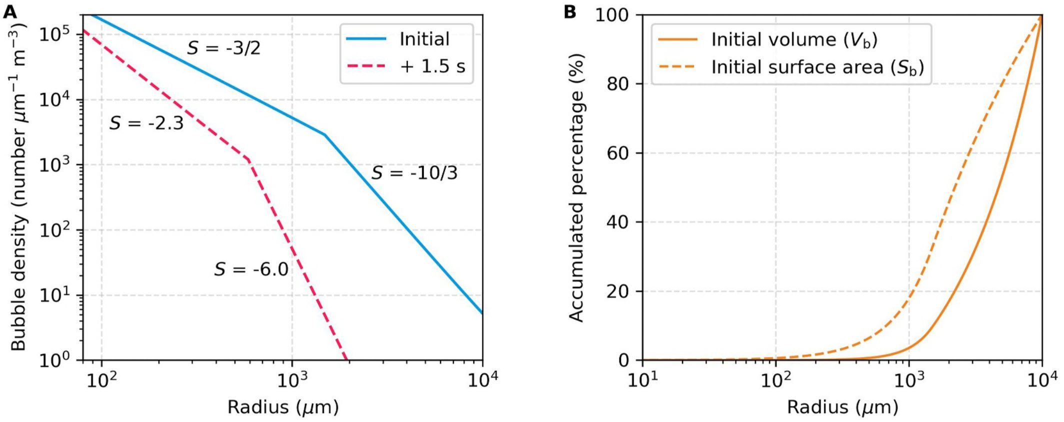

Figure 7. Examples of bubble size distributions measured in the wind-wave tank. (a) Bubble size distribution during a laboratory measurement (based on data from Deane & Stokes, 2002). Blue and red curves represent the bubble size distribution in the initial moment and 1.5 s later, respectively. Measurements in the coastal ocean show similar shapes (Deane & Stokes, 2002). (b) Accumulated bubble volume (solid line) and surface area (dashed line) as a percentage of the total, based on the initial bubble size distribution. The cutoff of maximum bubble diameter is set to 10^4 μm.

models, we briefly summarize the key aspects of bubble dynamics. Detailed treatments can be found in the literature listed in Table 1.

Wave breaking statistics. Wave breaking is the dominant mechanism for bubble generation in the surface ocean, and its statistics directly control air entrainment and, consequently, bubble-mediated gas exchange. Phillips (1985) proposed a framework of the length distribution of breaking crests, $\Lambda(c)$, to describe the wave breaking statistics, where c is the breaker phase speed. This framework was widely used (e.g., Banner et al., 2014; Deike & Melville, 2018; Sutherland & Melville, 2013) and recently reviewed by Deike (2022). In this framework, the zeroth through third moments of $\Lambda(c)$ correspond to the total breaking crest length, the surface area swept per unit time, whitecap coverage (W, defined as surface bubble patches following breaking; Monahan & O'Muircheartaigh, 1980), and the entrained bubble volume flux, respectively (Deike, 2022). The $\Lambda(c)$ is then scaled with the wind and wave parameters based on theoretical considerations and observations. This approach is used in the Deike and Melville (2018) model to simulate the bubble volume flux.

Bubble generation and initial bubble size distribution. After wave breaking, bubbles are generated through two primary physical mechanisms: (a) the jet and droplet entrainment interact with the wave face, yielding small bubbles; and (b) the air cavity trapped between the overturning jet and the wave face collapses under turbulent and shear flows, generating a fragmentation cascade that forms large bubbles (Deane & Stokes, 2002; Ruth et al., 2022). The Hinze scale (~1 mm; Hinze, 1955) separates the initial bubble size spectrum into super-Hinze and sub-Hinze regimes. Super-Hinze bubbles are fragmented by turbulence and follow a −10/3 power-law size distribution, whereas sub-Hinze bubbles are stabilized by surface tension and follow a −3/2 power-law size distribution (Deane & Stokes, 2002; Ruth et al., 2022). Together, these regimes define the initial bubble size distribution immediately after breaking (Figure 7a, blue curve). Although less numerous, super-Hinze bubbles dominate both bubble volume and surface area (Figure 7b; Goddijn-Murphy et al., 2016; Deike, 2022). Because the bubble size distribution exerts a first-order control on bubble-mediated transfer velocities and the solubility dependence of gas exchange (e.g., the transition solubility), it must be carefully represented in bubble models (see Section 2).

Bubble evolution. Active bubble generation is rapid, typically lasting ~1 s, after which bubbles organize into plumes. A shallow bubble plume layer forms within a few seconds following wave breaking and evolves under the combined effects of buoyant rise, turbulence-induced suspension, and gas dissolution, unless modified by surface-active materials (Deane & Stokes, 2002). Once active breaking ceases, the bubble spectrum evolves rapidly and steepens as plumes age (Figure 7a, red curve). This shallow layer is thought to dominate bubble-mediated gas exchange (Leighton et al., 2018). Shallow bubbles can be transported below 1 m by Langmuir circulation and turbulence (Czerski et al., 2022b; Liang et al., 2011; Sullivan & McWilliams, 2010). Small bubbles in deeper layers rise slowly and may dissolve completely, contributing to supersaturation of the least soluble gases (e.g., noble gases and O_2; Stanley et al., 2009; Deike et al., 2025), but having minimal impact on more soluble gases such as CO_2 (Keeling, 1993; Vagle et al., 2010; Woolf, 1993).

Key parameters during the bubble evaluation, including bubble penetration depth, rising speed, and single bubble gas transfer velocity, are also important in regulating bubble-mediated gas transfer (see Section 2), although these parameters remain poorly constrained. Bubble penetration depth is often parameterized as a function of wave breaking height based on laboratory experiments (e.g., Callaghan et al., 2013), but field observations reveal substantially more complex behavior (Benetazzo et al., 2024; Cifuentes-Lorenzen et al., 2023; Czerski et al., 2022a, Czerski et al., 2022b). Bubble rise speed is often estimated by the balance of the buoyancy and the friction, but recent studies suggest that it is also significantly controlled by the upper-ocean background turbulence (e.g., Ruth et al., 2021; Salibindla et al., 2020; Thorpe, 1984b). Finally, single bubble gas transfer velocities are sensitive to the presence of surfactants. Coated ("dirty") bubbles are expected to exhibit substantially lower transfer rates than "clean" bubbles (Woolf, 1993). However, the behavior of both "dirty" and "clean" bubbles remains poorly constrained due to a lack of sufficient field observations.

5.2. Physical Models

Early physical frameworks for bubble-mediated gas exchange were developed in the 1980s by Jähne et al. (1984) and Memery and Merlivat (1985). These studies highlighted both the solubility dependence of k_b and the bubble-induced asymmetric transfer. Building on these foundations, Woolf and Thorpe (1991) and Woolf (1993) explicitly coupled bubble and upper ocean water dynamics with gas exchange mechanisms, leading to the first physically based bubble model. The k_b from the model outputs was later parameterized by Woolf (1997), which shows theoretically expected asymptotic behavior: $k_b \propto Sc^{-0.5}$ for the least soluble gases, and $k_b = V_b/H$ for the more soluble gases (See Section 2), with a transition solubility near 1.5 (Figure 8a). This behavior is broadly supported by laboratory experiments (Mischler, 2014; Wanninkhof et al., 1995), although the transition solubility differs from laboratory estimates (Krall et al., 2019). Subsequent updates numerically resolved bubble plume dynamics and refined Δ_s using field bubble observations (Leighton et al., 2018) and were constrained by EC flux measurements (Dong et al., 2025). The bubble volume flux, V_b, is linearly linked with the wind speed-dependent W (Figure 8b) and the coefficient is constrained by laboratory observations (Cipriano & Blanchard, 1981). With the availability of EC CO_2 and DMS data (see Section 4), V_b, was further constrained, and the updated Woolf (1997) model has been incorporated into the COAREG gas transfer algorithm (Blomquist et al., 2017; Fairall et al., 2022).

An alternative and widely used physical model framework was developed by Keeling (1993) (see Section 2). Keeling (1993) focused exclusively on large bubbles (radius >500 μm), identifying them as the dominant contributors to bubble-mediated exchange, particularly for moderately soluble gases such as CO_2. The model predicts a single H–Sc scaling across all three poorly soluble gas categories (i.e., $k_b \propto H^{-0.3}Sc^{-0.35}$; Figure 8a), and therefore does not exhibit a transition solubility. The V_b in the Keeling (1993) model is also linked with W, but with a different parameterisation, which generates much lower V_b than that in the Woolf (1997) model. Based on the Keeling (1993) study, Deike and Melville (2018) and Deike et al. (2025) updated the model by incorporating a sea-state-dependent parameterisation of V_b with coefficients constrained by laboratory studies (Stanley et al., 2022) and EC observations (Figures 5 and 6). In the Deike et al. (2025) model, $k_b \propto H^{-0.35}Sc^{-0.5}$ (Figure 8a), while Δ_s scales approximately as $H^{-0.3}$. This updated model also explicitly accounts for fully dissolved bubbles, extending the original Keeling (1993) framework.

Liang et al. (2013) developed a bubble model using large-eddy simulations (Liang et al., 2011, 2012) that concurrently resolve upper-ocean turbulence, gas exchange at the bubble surface, gas fraction changes in bubbles, bubble size change, and bubble plume evolution. The parameterisation by Liang et al. (2013) was implemented in a global transport model and is shown to successfully reproduce observed deep-sea noble gas supersaturations. The global simulations also indicate comparable contributions from fully and partially dissolved bubbles for the least soluble gases, consistent with observations by Hamme and Emerson (2006). The Liang et al. (2013) parameterisation simulates only N_2 and O_2 exchange and assumes that k_b scales universally with $Sc^{-2/3}$, neglecting explicit solubility dependence.

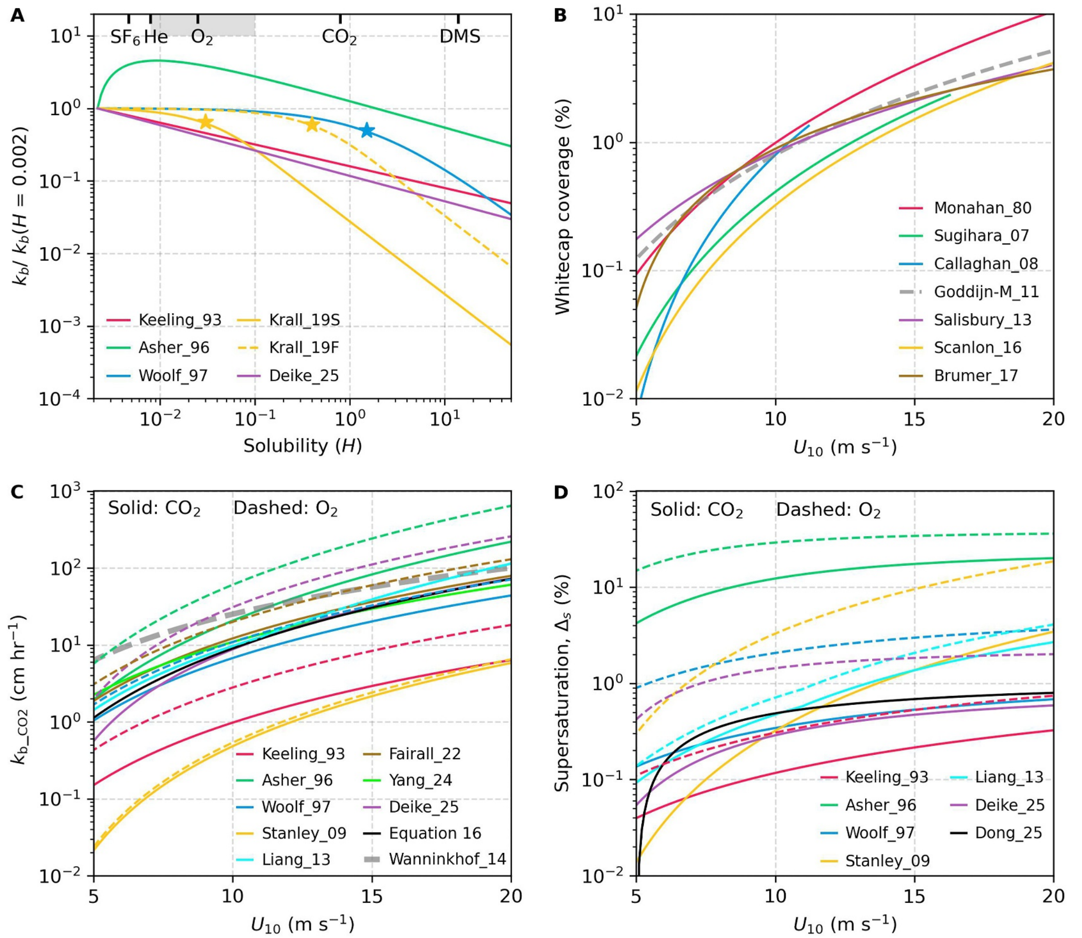

Figure 8. Bubble-mediated gas transfer velocity (k_b) and supersaturation (Δ_s) predicted by different models, together with whitecap coverage (W) parameterizations. (a) Dependence of the relative k_b on gas solubility (H). For each model, k_b is normalized by its value at $H = 0.002$. Solubilities of several gases are indicated above the panel, and the gray shadow represents the solubility range of the noble gases at 20°C. Stars denote the transition solubility for each model. Solid and dashed yellow lines show the Krall et al. (2019) model for seawater and freshwater, respectively. (b) Selected parameterizations for W (%, See Table A9 for references). (c) k_b values for CO_2 (solid lines) and O_2 (dashed lines) from different models (See Table A8 and the main text for model details). The Goddijn-Murphy et al. (2011) parameterization (gray dashed line in b) is applied to all models that require W. Evasion transfer velocities are shown for all models. The Krall et al. (2019) model predicts $k_b = 0$ over the wind-speed range considered and is therefore not visible on the logarithmic y-axis. The black line shows Equation 16 (constrained by EC data), and the dashed gray line indicates the Wanninkhof (2014) parameterization for k for reference. (d) Δ_s (%) for CO_2 (solid lines) and O_2 (dashed lines). Estimation of Δ_s requires an interfacial component, and the DMS transfer velocity shown in Figure 5B is used consistently across models. The Woolf (1997) results reflect the updated formulation of Leighton et al. (2018).

5.3. Empirical Models

Empirical models adopt the basic air-sea gas exchange frameworks (see Section 2) and constrain bubble effects using laboratory or field observations (see Sections 3 and 4), without numerically resolving bubble dynamics. These models can be broadly grouped into three categories based on the observational constraints employed: (a) laboratory measurements of gas transfer velocities across a range of gas solubilities, (b) field observations of gas saturation states, and (c) field EC observations of CO_2 and DMS transfer velocities.

Building on the frameworks of Memery and Merlivat (1985) and Keeling (1993), Asher et al. (1996) expressed k_b as a function of solubility and Schmidt number with several unknown coefficients, which were statistically constrained using laboratory measurements of gas transfer velocities spanning a wide range of solubilities (see Section 3.2). Separate invasion and evasion experiments are conducted to isolate bubble-induced asymmetry. Because these experiments employed artificially introduced bubbles generated by a tipping bucket, without wind forcing, the bubble volume flux scaled linearly with observed W in the tank. Using empirical relationships between W and wind speed in the field (Figure 8b), the laboratory results were converted to wind-speed-dependent parameterizations (Figures 8c and 8d). While the model reproduces the laboratory data well, the fitted coefficients imply an unphysical negative contribution from small bubbles and predict a decrease in k_b for the least soluble gases (Figure 8a). Moreover, the large invasion-evasion asymmetry inferred from the experiments leads to extremely large values of Δ_s (Figure 8d). An alternative empirical framework was developed based on laboratory experiments by Mischler (2014) and Krall et al. (2019) (Sections 3.2 and 3.4). Mischler (2014), using a bubble-injection tank, observed the theoretically expected asymptotic behavior: $k_b \propto Sc^{-0.5}$ for the least soluble gases, and $k_b \propto H^{-1}$ for more soluble gases. Krall et al. (2019) incorporated this H and Sc dependence and constrained the transition solubility, H_t, and V_b using experimental results. The experiment was conducted in linear wind-wave tanks, where bubbles were generated by hurricane-strength wind-driven wave breaking. Separate constraints were derived for freshwater and seawater, revealing a higher H_t in seawater due to differences in bubble size distributions (Figure 8a). The Krall et al. (2019) model predicts negligible bubble volume flux (Figure A3) and thus minimal bubble-mediated transfer velocities for all gases under typical oceanic wind conditions (i.e., 0–20 m s^{-1}).

Field observations of noble gas supersaturation and temporal variability in dissolved N_2 and O_2 (see Section 4.1) provide an additional means to constrain empirical bubble models. Stanley et al. (2009) adopted the Keeling (1993) framework, partitioning the gas exchange into interfacial transfer and bubble-mediated transfer from fully and partially dissolved bubbles. The interfacial transfer is then represented using a ^{14}C-based parameterization (Wanninkhof, 1992), and the two bubble components are tuned using timeseries of five noble gas saturations with the mass balance method. Similar approaches were applied by Nicholson et al. (2011) using expanded noble gas data sets, by Vagle et al. (2010) based on near-surface N_2 and O_2 observations, and by Ito et al. (2011) using global mean Ne supersaturation data. Because these studies rely on different data sets and modeling assumptions, the inferred partitioning between fully and partially dissolved bubble contributions, as well as the resulting supersaturation estimates, varies substantially among models (see Liang et al., 2013).

The availability of EC CO_2 and DMS observations (see Section 4.2) provides a direct constraint on the bubble effect for gases with solubilities similar to CO_2. Yang et al. (2024) used a least-squares method to separate interfacial (k_i) and bubble-mediated (k_b) components from EC-derived CO_2 transfer velocities. The constrained k_i closely matches observed DMS transfer velocities, while the derived k_b agrees well with estimates based on observed CO_2-DMS differences (Equation 16; Figure 8c). Dong et al. (2025) further constrained Δ_s for CO_2 by combining EC-derived k_i and k_b with the overpressure factor obtained from bubble observations and a physical bubble model (Leighton et al., 2018; Figure 8d). Since the EC technique only works for the two poorly soluble gases at the moment, these constraints cannot resolve solubility dependence.

5.4. Uncertainties of the Models

Taken together, the wide spread among model predictions in Figure 8 highlights the substantial uncertainties that remain in current simulations of bubble-mediated gas exchange. The transition solubility inferred from empirical and physical models spans one and a half orders of magnitude (Figure 8a), while the simulated k_b and Δ_s (after normalizing the whitecap coverage) vary by roughly an order of magnitude for both CO_2 and O_2, even when excluding extreme outliers (Figures 8c and 8d). However, it should be noted that some earlier parameterizations have been refined or superseded by more recent studies with improved observational and mechanistic constraints (see Sections 5.2 and 5.3). If only models developed or substantially updated in the past decade are considered, the spread in predicted k_b and Δ_s becomes considerably smaller, with many recent estimates converging within approximately half an order of magnitude (Figures 8c and 8d).

Models that numerically resolve bubble plume dynamics are often described as physical models, but they are not independent of observations and require several poorly constrained inputs, including the initial bubble size distribution and bubble volume flux. Recent advances in dynamic bubble modeling (e.g., Deike, 2022; Liang et al., 2013) and emerging frameworks linking laboratory and model results (Deike et al., 2025) are encouraging, although important uncertainties remain. Laboratory measurements of bubble size distributions are commonly adopted. However, direct field support for these choices remains limited due to the difficulty of observing bubbles in the near-surface ocean. Most field measurements capture bubble plumes tens to hundreds of seconds after wave breaking and at depths below the surface layer, rather than the initial near-surface distributions that are most relevant for gas exchange (e.g., Czerski et al., 2022a, Czerski et al., 2022b; Graham et al., 2004; Medwin & Breitz, 1989; Monahan & Lu, 1990; Thorpe, 1984a; Thorpe et al., 1992). Because bubble size distributions strongly influence the H and Sc dependence of bubble-mediated transfer, their uncertainties propagate directly into large uncertainties in modeled solubility scaling (Figure 8a). The bubble volume flux is another major source of uncertainty, as it directly sets the magnitude of bubble-mediated exchange. In most models, V_b is parameterized using W derived from field observations, yet existing wind speed-related parameterizations of W differ widely (Figure 8b). Increasing evidence suggests that wind speed alone is insufficient to describe W, which also depends on sea states (e.g., Brumer, Zappa, Blomquist, et al., 2017; Deike, 2022). Moreover, translating W into an actual bubble volume flux introduces additional uncertainty, which largely explains the magnitude difference of k_b and Δ_s predicted by Woolf (1997) and Keeling (1993) models (Figures 8c and 8d). Additional uncertainties that are not reflected in Figure 8 are the "clean" or "dirty" bubble assumption, since all models mentioned above assume that bubbles are clean. However, surfactant coatings can dampen single bubble transfer velocity, and the surfactants produced by the phytoplankton are ubiquitous in the ocean environment (e.g., Wurl et al., 2011). The bubble-mediated gas transfer in physical models is highly sensitive to surfactants, which limits the applicability of "clean" bubble models to natural ocean conditions (e.g., Czerski et al., 2022b; Woolf, 1993). These uncertainties highlight the urgent need for improved in situ bubble measurements to refine and validate these models.

Empirical models constrained by field observations of specific gases (e.g., EC CO_2 and DMS observations) have provided valuable constraints on the magnitude of bubble-mediated exchange for gases with similar solubilities (e.g., Bell et al., 2017; Blomquist et al., 2017; Dong et al., 2025). However, these parameterizations generally do not explicitly resolve the solubility dependence of the bubble-mediated gas exchange and may not be directly transferable to gases with substantially different solubilities. Laboratory experiments can overcome this limitation by using gases spanning a wide range of solubilities, but scaling laboratory results to the open ocean remains challenging. Bubble concentrations measured in an annular wind-wave tank with effectively infinite fetch are approximately an order of magnitude higher than those observed in fetch-limited linear wind-wave tanks under comparable wind speeds (Figure A4; Flothow, 2017). The substantially lower bubble production in linear tanks likely contributes to the weak bubble effects predicted by the Krall et al. (2019) model. Consistent with this interpretation, the bubble volume flux in the Krall et al. (2019) model is roughly 1.5 orders of magnitude smaller than that in the Woolf (1997) model at equivalent wind speeds. More generally, differences in water depth, fetch, and flow dynamics between laboratory facilities and the open ocean complicate direct extrapolation, and robust scaling relationships have yet to be established.

6. Knowledge Gaps and Priorities for Future Study

Substantial progress has been made over recent decades in understanding the properties of bubble-mediated gas exchange and quantifying its role across gases with different solubilities. However, each section of this review has also identified significant limitations and sources of uncertainty in current observations and model simulations. Here, we identify basic agreements and disagreements and key knowledge gaps, and outline key priorities for future research aimed at improving the robustness and generality of bubble-mediated gas exchange frameworks.

6.1. Agreements and Disagreements

A central question of the reviewed topic is whether bubbles play a significant role in air-sea gas exchange. Because it is well agreed that bubble-mediated gas exchange is solubility dependent, the answer varies across gases. For the least soluble gases, such as O_2, there is broad agreement that bubbles make an important contribution to their exchange. However, the magnitude remains uncertain, and estimates of the bubble-mediated O_2 transfer velocity span nearly an order of magnitude, ranging from comparable to interfacial transfer to dominating the total exchange at U_{10} of $\sim$15 m s^{-1} (Figure 8c). For the soluble gases within the poorly soluble category, such as DMS, existing evidence consistently indicates that bubble effects are negligible and observed transfer velocities largely reflect solubility-independent interfacial exchange.

For moderately soluble gases, such as CO_2, the role of bubbles remains strongly debated. Laboratory experiments with sufficiently intense artificial bubble introduction show substantially higher transfer velocities for gases with CO_2-like solubilities than for more soluble gases. In contrast, linear wind-wave tank experiments with wind-driven breaking and natural bubble generation show minimal bubble enhancement for CO_2 (Section 3). Field EC CO_2 and DMS observations generally support a significant bubble contribution to air-sea CO_2 exchange, yet at least one cruise does not show a significant difference in the observed transfer velocities between CO_2 and DMS (Section 4). Moreover, it is still unclear why CO_2 transfer velocities are not substantially lower than SF_6 and ^3He (the two least soluble gases) from the dual-tracer field experiment. Model estimates of bubble-mediated CO_2 transfer velocity span roughly an order of magnitude, from negligible to comparable with interfacial exchange at U_{10} of ∼15 m s^{-1} (Figure 8c).

Worth noting again that the classifications "the least soluble," "moderately soluble," and "soluble" (Table 1) used in this review are relative terms, all referring to poorly soluble gases.

6.2. Key Knowledge Gaps

The disagreements over moderately soluble gases, together with the wide spread in the quantification for both the least soluble and moderately soluble gases, indicate that major knowledge gaps remain in our understanding of bubble-mediated air-sea gas exchange.

Bubble dynamics and the transition solubility: Although it is well established that bubble-mediated exchange depends on gas solubility, the functional form of this dependence remains uncertain (Figure 8a), limiting our ability to scale bubble effects across gases. Theory and laboratory studies suggest the existence of a transition solubility, H_t, above which transfer is strongly solubility dependent and below which it depends primarily on the Schmidt number. However, existing models predict values of H_t differing by orders of magnitude, which is particularly relevant for CO_2. If H_t is much lower than the solubility of CO_2, then the bubble-mediated transfer velocity follows $k_b = V_b/H$ (Equation 14), and the importance of bubbles for CO_2 exchange depends almost entirely on the bubble volume flux. For instance, at U_{10} of ∼15 m s^{-1}, the interfacial transfer velocity is ∼30 cm hr^{-1} based on DMS observations (Figure 5b), and bubble-mediated transfer would become comparable if V_b reached roughly 0.5 L per m^2 sea surface area per second. In contrast, if H_t exceeds the solubility of CO_2, then k_b for CO_2 only has a weak solubility dependence and instead scales mainly with the Schmidt number, which may help explain why observed CO_2 transfer velocities are similar to those of the least soluble gases (i.e., $SF_6/^3He$). The large difference in modeled solubility dependence H_t (Figure 8a) ultimately reflect limited understanding of bubble dynamics (Equations 13–15). Most required bubble dynamic inputs in the physical bubble model are based on laboratory measurements, while field constraints on the three-dimensional bubble size distribution remain sparse. Critical gaps include the initial near-surface bubble size spectrum and volume flux, bubble evolution under realistic upper-ocean turbulence and wave fields, and the gas transfer behavior of individual bubbles under natural conditions.

Consistent field constraints across solubility categories: At present, coherent quantifications of bubble-mediated transfer across all three poorly soluble gas categories come mainly from physical bubble models or laboratory experiments using multiple gases. Field observations, in contrast, tend to constrain either the least soluble gases (via gas saturation data) or moderately soluble gases (via EC data). In principle, combining the saturation measurements with EC-based CO_2 and DMS transfer velocity observations could provide a field constraint across solubility categories. However, achieving this requires simultaneous application of both techniques and a careful translation between the supersaturation-based and the transfer velocity-based quantifications. Such coordinated measurement and synthesis studies remain largely absent.

Scaling from laboratory to the field: Laboratory experiments have been essential for understanding bubble dynamics and quantifying the solubility dependence of bubble-mediated transfer, yet quantitatively scaling laboratory results to oceanic conditions remains challenging and not straightforward. Bubble simulation tanks cannot mimic oceanic wave breaking and bubble generation processes. Linear wind-wave tanks lack the fetch needed to replicate open-ocean wave breaking at equivalent wind speeds, although wave paddles partially compensate by generating more realistic wave spectra. Fetch-unlimited annular tanks produce bubble concentrations about an order of magnitude larger than linear facilities at comparable wind (Figure A4), indicating that fetch strongly controls bubble production. However, annular tanks still face a shallow water depth (∼1 m), which also affects wave breaking and the deep bubble penetration. In addition, differences in upper-ocean turbulence and Langmuir circulation between tanks and the ocean affect bubble penetration and residence times. These discrepancies complicate direct extrapolation of laboratory-based parameterizations, and robust scaling frameworks linking laboratory, model, and field conditions have yet to be established.

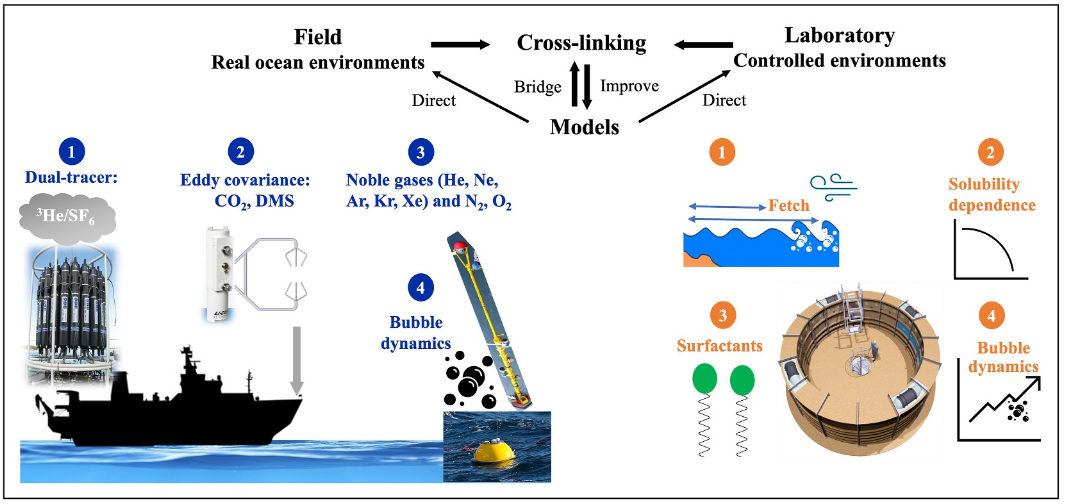

Figure 9. Cross-linking laboratory experiments, field observations, and models to improve quantification of bubble-mediated air-sea gas transfer across gases with different solubilities.

6.3. Priorities for Future Study

Air-sea gas exchange plays a central role in regulating Earth's climate and ocean biogeochemistry. Accurate estimates of global CO_2 and O_2 fluxes are essential for predicting climate change and marine ecosystem responses. In addition, the emergence of mCDR applications requires a robust mechanistic understanding of gas exchange processes, particularly the role of bubbles in CO_2 transfer, to quantify additionality and durability. Recent studies indicate that bubble-mediated transfer may account for ~40% of the global ocean CO_2 flux (Reichl & Deike, 2020). Bubble-induced asymmetry may enhance global ocean CO_2 uptake by ~15% (Dong et al., 2025) and reduce global ocean O_2 loss by ~25% (Deike et al., 2025). Explicitly accounting for wave and bubble processes can alter local CO_2 flux estimates by 20%–50% relative to wind-only parameterizations (Rustogi et al., 2025), while neglecting bubble effects may underestimate O_2 uptake in regions such as the Labrador Sea by up to an order of magnitude (Atamanchuk et al., 2020). These results underscore the importance of resolving bubble processes for both regional and global budgets.

To address the key knowledge gaps and improve our capacity to quantify bubble-mediated air-sea gas exchange, we identify the following priorities for future research.

Comprehensive high-wind field campaigns: Future campaigns under strong wind and wave conditions should prioritize measurements of near-surface bubble and upper-ocean dynamics. Targeted observations of bubble size distributions, vertical transport, evolution, whitecap coverage, and the single bubble transfer velocity are essential for improving physical bubble models. Concurrently, air-sea exchange of gases spanning a wide range of solubilities should be measured using multiple complementary techniques, including dual-tracer experiments, EC, and gas saturation measurements (Figure 9). Such coordinated data sets will enable integrated, field-based assessment of bubble contributions across solubility regimes.

Bridging laboratory and field observations: Controlled experiments in wind-wave tanks should explicitly investigate the roles of fetch and water depth in regulating bubble generation, size spectra, and volume fluxes. A mechanistic understanding from laboratory studies, combined with a systematic comparison to field observations, is necessary to establish scaling frameworks that translate laboratory results to oceanic conditions and reconcile discrepancies among different facilities and the open ocean. Numerical models and simulations are also important tools for integrating process understanding and developing robust laboratory-to-field scaling frameworks. Moreover, the controlled conditions and high precision of laboratory experiments enable rigorous quantification of bubble-induced asymmetry, for example, through simultaneous measurements of invasive gas transfer velocities and supersaturation. Such measurements are essential for constraining Δ_s and for improving estimates of global ocean CO_2 and O_2 flux budgets.

Improved modeling frameworks: New near-surface field observations should be used to refine representations of bubble dynamics in models to improve the simulation of both the solubility dependence and magnitude of bubble-mediated exchange. Because bubble concentration and whitecap coverage do not directly provide volumetric flushing and injection rates, coupled fluid-dynamical modeling is also required to resolve bubble volume fluxes and plume evolution more realistically. Moreover, the development of a unified modeling framework that links saturation-based constraints for the least soluble gases with EC-based constraints for moderately and highly soluble gases is needed, which would enable the prediction of bubble-mediated transfer across the full solubility spectrum using field data.

Advancing sensor techniques: The EC technique has been successfully applied to CO_2 (moderately soluble) and DMS (soluble). Extending EC instruments to accurately measure the least soluble gases (e.g., CH_4 and O_2) at high frequency would enable characterization of bubble-mediated gas transfer across the full solubility range using a consistent field methodology. Further advances in sensor technology that allow sustained near-surface observations of bubbles, dissolved gases, and EC fluxes under extreme ocean conditions will substantially enhance observational coverage and model validation.

Appendix A

Table A1

Table A1
Comparison of the Woolf (1993) and Keeling (1993) Frameworks and Their Translation

Models	Woolf and Thorpe (1991); Woolf (1993, 1997)	Keeling (1993)	Translation
Total and bubble-mediated gas flux	$F = (k_i + k_b)\left[C_w - (1 + \Delta_s)C_a\right]$; $F_b = k_b[C_w - (1 + \delta)HC_a]$	$F = \left(k_i + k_b^{\text{out}}\right)(C_w - C_a) - \left(k_b^{\text{in}} - k_b^{\text{out}}\right)C_a$; $F_b = k_b^{\text{out}}C_w - k_b^{\text{in}}HC_a$	$k_b = k_b^{\text{out}}$; $k_b^{\text{in}} = (1 + \delta)k_b$; $\Delta_s = \left(k_b^{\text{in}} - k_b^{\text{out}}\right)/\left(k_i + k_b^{\text{out}}\right)$; $\Delta_s = \delta k_b/(k_i + k_b)$
Physical expression of k_b	$k_b = V/H$, $(H \gg 1)$; $k_b \propto Sc^{-1/2}$ $(H \ll 1)$	$k_b^{\text{out}} = V_{\text{exch}}/H$; $k_b^{\text{in}} = V_{\text{exch}}/H + V_{\text{inj}}/H + (\Delta P V_{\text{exch}})/(PH)$;	$V_{\text{exch}} = VE(r)$
Calculation of the supersaturation factor	$\Delta_s = \delta k_b/(k_i + k_b)$	$\Delta_s = \left(k_b^{\text{in}} - k_b^{\text{out}}\right)/\left(k_i + k_b^{\text{out}}\right)$	$\delta = \left(k_b^{\text{in}} - k_b^{\text{out}}\right)/k_b^{\text{out}}$
Individual bubble transfer velocity[a]	Various including $k_{sb} = [(1 - 2.89/\sqrt{Re})(2DU)/(r\pi)]^{1/2}$, Re > 10 for large bubbles	$k_{sb} = [(2DU)/(r\pi)]^{1/2}$	Differences in detail
Characteristic bubble depth	Modeled depth ~0.25 cm	0.25 cm ("best" guess)	Broadly consistent
Bubble flux	$V = \int 4\pi r^3 Q(r)\,dr/3$	$V_{\text{exch}} = \int 4\pi r^3 Q(r)E(r)\,dr/3$; $E(r) = z_0(r)/(z_0(r) + H_{eq}(r))$; $H_{eq}(r) = rU(r)/(3Hj(r))$	$V_{\text{exch}} = VE(r)$
Parameterisation of bubble flux by the whitecap	$V = 2450W_B$ cm h^{-1}	$V = 3600W_A$ cm h^{-1} (The "best" guess); $W_B \approx 10W_A$	Neither has adequate field data support
H and Sc dependence of k_b	$k_b = 2450W_B\left[1 + \left(1.4HSc^{-1/2}\right)^{-1/1.2}\right]^{-1.2}/H$	$k_b = 3600W_a\left(3.5H^{0.7}Sc^{-0.35}\right)/H$	Key difference
H and Sc dependence of Δ	Dependences on H, but no simple rule	$\Delta_s \propto H^{-0.3}$	Both rely on model outputs

[a]The individual bubble transfer velocity in the Keeling framework, $k(r)$, is defined differently from that in the Woolf framework, j, with the relation $k(r) = 4\pi j$. For consistency, we express both frameworks using k_{sb}, which is equal to j.

Table A2

Table A2
Gas Solubility and Schmidt Numbers in Seawater at 20°C (Salinity = 35‰)[a]

Gas name	Chemical formula	Solubility (H)	Schmidt number (Sc)
Sulfur hexafluoride[b]	SF_6	0.004	992
Carbon tetrafluoride[c]	CF_4	0.005	812
Helium-3[b]	^3He	0.008	144
Helium[b]	He	0.008	165
Neon[b]	Ne	0.009	315
Nitrogen[b]	N_2	0.012	670
Hydrogen[d]	H_2	0.019	194
Hydrogen deuteride[d]	HD	0.020	239
Deuterium[d]	D_2	0.020	275
Oxygen[b]	O_2	0.025	589
Methane[b]	CH_4	0.028	677
Argon[b]	Ar	0.028	576
Krypton[b]	Kr	0.050	694
Pentafluoroethane (PFE)[c]	CF_3CHF_2	0.07	1030
Xenon[b]	Xe	0.10	880
Radon[b]	Rn	0.32	980
Nitrous oxide[b]	N_2O	0.52	698
Carbon dioxide[b]	CO_2	0.73	660
Acetylene[c]	C_2H_2	0.91	686
Hexafluorobenzene (HFB)[c]	C_6F_6	1.10	1360
Difluoromethane[c]	CH_2F_2	1.50	818
Chloromethane[d]	CH_3Cl	2.55	714
1,4-Difluorobenzene (DFB)[c]	$C_6H_4F_2$	3.10	1230
Bromomethane[e]	CH_3Br	3.85	700
Benzene[d]	C_6H_6	4.40	909
Dimethyl sulfide (DMS)[b]	$(CH_3)_2S$	12.7	918
Anisole[f]	$C_6H_5OCH_3$	89.9	1514
Methyl acetate (MA)[c]	CH_3COOCH_3	150	856

[a]Values are from disparate sources and should be considered approximate (∼5%). [b]From (Wanninkhof et al., 2009) for seawater. [c]From Krall et al. (2019) for freshwater. [d]From Mischler (2014) for freshwater. [e]Calculated from empirical equations given by De Bruyn and Saltzman (1997a, 1997b). [f]Calculated from empirical equations given by Sander (2023) for H and Yaws (2009) for Sc.

Selected laboratory experiments on bubble-mediated gas exchange in different types of wave tanks (Table A3–A6).

Table A3

Table A3
Linear Wind-Wave Tanks (Limited Wind Speed Capacity)

Studies	Broecker and Siems (1984)	Merlivat and Memery (1983); Memery and Merlivat (1984)	Jähne et al. (1984)	Bowyer and Woolf (2004); Rhee et al. (2007); Woolf et al. (2007)
Facility	Hamburg	Marseille-small	Marseille-large (LASIF)	
Tank type	Linear wind-wave tank			
L, W, H	24 m, 1.0 m, 1.5 m	8 m, 0.5 m, 0.6 m	40 m, 2.6 m, 2.4 m	
Reference wind speed[a]	0–24 m s^{-1}	0–15 m s^{-1}	0–14 m s^{-1}	
Gases used	O_2, CO_2	Ar, N_2O	He, Rn	SF_6, He, CH_3Br, N_2O, air
Water type	Freshwater	Fresh and seawater	Freshwater	Freshwater
Bubble generation method	Wind-driven wave breaking	Wind-driven and mechanically generated wave breaking	Wind-driven wave breaking	Wind-driven and paddle-generated wave breaking; Artificial bubbles pumped by aeration
Invasion or evasion	Evasion	Invasion	Evasion	Invasion and evasion
Measure bubbles?	Yes	No	Yes	Yes
Notes	• k increases sharply at high wind speeds, with a notable divergence between $k_{\_O2}$ and $k_{\_CO2}$; • Bubble surface area approaches the sea-surface area under high winds.	• No consistent differences were observed between $k_{\_Ar}$ and $k_{\_N2O}$; • k shows no significant difference between freshwater and seawater.	• k_{660_He} and k_{660_Rn} exhibit no significant differences; • Bubble concentrations were very low even under the tank's maximum wind speed.	• k did not show solubility dependence without artificially introduced bubbles; • k exhibited clear solubility dependence when artificial bubbles were pumped.

[a]Wind speeds in different facilities are not directly comparable and not equivalent to wind speeds in the ocean.

Table A4

Table A4
Bubble Simulation Tanks (No Wind)

Studies	Asher et al. (1995); Wang et al. (1995); Wanninkhof et al. (1995)	Asher et al. (1996); Leifer et al. (1995)	Mischler (2014)
Facility	California	Washington	Heidelberg
Tank type	Surf pool	Whitecap simulation tank	Bubble simulation tank
Length, Width, Depth	70 m, 20 m, 0.8 m	1.2 m, 1.2 m, 1.8 m	1.3 m, 0.15 m, 0.7 m
Reference wind speed range	No wind	No wind	No wind
Gases used	SF_6, He, N_2O, CO_2	SF_6, He, O_2, CO_2, DMS	SF_6, Ne, N_2, HD, D_2, O_2, Kr, CF_3CHF_2, Xe, N_2O, C_2H_2, CH_3Cl, C_6H_6, DMS
Water type	Freshwater	Seawater	Fresh and artificial seawater
Bubble generation method	Mechanically generated wave breaking	Water release by tipping bucket	Water jet
Invasion or evasion	Evasion	Invasion and evasion	Invasion and evasion
Measure bubbles	Yes	Yes	Yes
Notes	• k shows clear solubility dependence; • The Woolf (1997) model reproduces observed results reasonably well; • The Keeling (1993) model overestimates solubility dependence and overpredicts N_2O exchange.	• Bubbles play a significant role in gas exchange; • Invasion fluxes are more efficient than evasion, and this asymmetry weakens with increasing solubility; • k_b is linked to whitecap coverage, and an empirical model was developed.	• k depends on Schmidt number (solubility) for gases with solubility lower (higher) than the transition solubility; • The transition solubility ranges from 0.04 for seawater to 0.44 for freshwater; • k is substantially higher in seawater than in freshwater; • Evasion experiments were unsuccessful.

Table A5

Table A5
Annular Wind-Wave Tanks (Unlimited Fetch)

Studies	McGillis et al. (1995)	Flothow (2017)
Facility	**Woods Hole**	**Heidelberg (Aeolotron)**
Tank type	Annular wind-wave tank (unlimited fetch)	
Diameter, flume width, height	0.25 m, 0.1 m, 0.1 m	10 m, 0.6 m, 2.4 m
Reference wind speed range	Air friction velocity (u_{*a}): 0–6 cm s^{-1}	0–24 m s^{-1}
Gases used	O_2	None
Water type	Fresh and seawater	Fresh and artificial seawater
Bubble generation method	Wind-driven wave-breaking and bubble-pumping	Wind-driven wave breaking
Invasion or evasion	Invasion and evasion	None
Measure bubbles	Yes	Yes
Notes	• Bubble-mediated gas transfer is significant when artificial bubbles are injected or the wind speed is high; • k_b is greater in seawater than in freshwater; • Calculated k is greater for invasion than evasion at high wind in the wind-driven wave breaking condition.	• The bubble surface area and the bubble volume are ~ an order larger than in the linear wind-wave tank under the same reference wind speed;

Table A6

Table A6
Linear Wind-Wave Tanks (Very High Wind Speed Capacity)

Studies	Iwano et al. (2013); Krall and Jähne (2014); Krall et al. (2019)	Krall et al. (2019)	Stanley et al. (2022)
Facility	Kyoto	Miami (SUSTAIN)	Miami (SUSTAIN)
Tank type	Linear wind-wave tank		
Length, width, height	16 m, 0.8 m, 1.6 m	24 m, 6 m, 2 m	24 m, 6 m, 2 m
Reference wind speed	7–67 m s^{-1}	14–85 m s^{-1}	10–50 m s^{-1}
Gases used	CF_4, SF_6, He, C_2HF_5, Xe, C_6H_6, CO_2, CH_2F_2, $C_6H_4F_2$, DMS, CH_3COOCH_3	SF_6, He, Kr, C_2HF_5, C_2H_2, C_6H_6, CH_2F_2, DMS, CH_3COOCH_3	He, Ne, Ar, Kr, Xe
Water type	Fresh and artificial seawater	Seawater	Seawater
Bubble generation method	Wind-driven wave breaking	Wind-driven wave breaking	Wave breaking resulting from wind stress acting on the paddle-generated background waves
Invasion or evasion	Evasion	Evasion	Invasion/evasion
Measure bubbles	Yes	No	Yes
Notes	• Observed k increases sharply at wind speeds above 33–34 m s^{-1}; Under extreme winds, k reaches values orders of magnitude higher than in typical ocean conditions; • No clear solubility dependence of k is seen at equivalent 10-m wind speed below 33 m s^{-1}; Solubility dependence emerges at high wind speeds in seawater, but remains negligible in freshwater; Bubble effects on moderately soluble and soluble gases are minimal under all conditions. • The total transfer velocity measured could be split up into bubble volume related, bubble surface area related, and water surface related transfer		• Supersaturation is detectable at equivalent 10-m wind speeds as low as 10 m s^{-1}; • Supersaturation increases with wind speed initially, then plateaus at higher speeds; • Invasion fluxes exceed evasion fluxes under otherwise similar conditions.

Table A7

Table A7
Selected Eddy Covariance Air-Sea DMS[a] and CO_2 Exchange Observations With Air Drying Setup

Cruise	Time	Location	Gas	Bubble meas.?	Reference
TAO	Nov 2003	Equatorial Pacific	DMS	No	Huebert et al. (2004)
PHASE I	May–July 2004	North Pacific	DMS	No	Marandino et al. (2007)
BIO	Summer 2004	Sargasso Sea	DMS	No	Blomquist et al. (2006)
Knorr06	Jan 2006	South-east Pacific	DMS	No	Marandino et al. (2009)
DOGGE	June–July 2007	North Atlantic	DMS	No	Huebert et al. (2010); Salter et al. (2011)
Knorr07	May–July 2007	North Atlantic	DMS, CO_2 (inv)	No	Marandino et al. (2008); Miller et al. (2009, 2010)
SO GasEx[b]	Feb–Apr 2008	Southern Ocean	DMS, CO_2 (inv)	No	Edson et al. (2011); Yang et al. (2011)
VOCALS	Oct–Nov 2008	Southeast Pacific	DMS	No	Yang et al. (2009)
Knorr11	June–July 2011	North Atlantic	DMS, CO_2 (inv)	No	Bell et al. (2013, 2017)
SOAP	Feb–Mar 2012	Southern Ocean	DMS, CO_2 (inv)	No	Bell et al. (2015); Landwehr et al. (2018)
NBP	Jan–Feb 2013; Feb–Mar 2014	Southern Ocean	CO_2 (inv)	No	Butterworth and Miller (2016)
HiWinGS	Oct–Nov 2013	North Atlantic	DMS, CO_2 (inv)	Yes	Blomquist et al. (2017)
SONNE	July–Aug 2014	Tropical Indian	DMS, CO_2 (inv/eva)	No	Zavarsky et al. (2018)
AMT28	Oct 2018	Tropical Atlantic	CO_2 (inv/eva)	No	Dong, Yang, Bakker, Liss, et al. (2021); Ford et al. (2024)
JR18004	Jan–Feb 2019	Southern Ocean	CO_2 (inv)	No	Dong et al. (2024)
ANDREXII	Feb–Apr 2019	Southern Ocean	CO_2 (inv/eva)	No	Yang et al. (2021)
JR18007	Aug–Sep 2019	Arctic Ocean	CO_2 (inv)	No	Dong, Yang, Bakker, Kitidis, and Bell (2021)
AMT29	Nov 2019	Tropical Atlantic	CO_2 (inv/eva)	No	Dong, Yang, Bakker, Liss, et al. (2021); Ford et al. (2024)
JR19001	Nov–Dec 2019	Southern Ocean	CO_2 (inv)	No	Dong et al. (2024)
JR19002	Jan–Feb 2019	Southern Ocean	CO_2 (inv)	No	Dong et al. (2024)
JR30001	Nov–Dec 2020	Southern Ocean	CO_2 (inv/eva)	No	Dong et al. (2024)

[a]DMS fluxes are always evasive. [b]CO_2 measurements are unreasonable (factor of 10 higher than expected) due to the water vapor sensitivity.

Table A8

Table A8
Bubble-Mediated Gas Transfer Models

References of models	Model type	H and Sc dependence of k_b	Notes
Jähne et al. (1984)	Physical	–	• Propose the equilibrating time and bubble lifetime
Memery and Merlivat (1985)	Physical	–	• Framework for developing a bubble model
Woolf and Thorpe (1991); Woolf (1993, 1997)	Physical	$\propto H^{-1}$, $H \gg H_t$; $\propto Sc^{-0.5}$, $H << H_t$;	• First k_b model with physical bubble dynamics; • Applicable to the ocean and the full range of solubilities • Blomquist et al. (2017) and Fairall et al. (2022) Use the Woolf model, but constrained the bubble volume flux use the EC DMS and CO_2 data
Keeling (1993)	Physical	$\propto H^{-0.3}Sc^{-0.35}$	• Large bubbles are important for k_b, the model only considers large bubbles

Table A8
Continued

References of models	Model type	H and Sc dependence of k_b	Notes
Asher et al. (1996)	Empirical	$\propto (aH^{-1} + bH^{-0.37}Sc^{-0.18})$	• Constrained by laboratory experiments; • Provide different parameterizations of k_b for invasion and evasion
Stanley et al. (2009)	Empirical	–	• Constrained by the observed supersaturation of noble gases at the Bermuda Atlantic Times-series Study (BATS) site; • Fully dissolving bubbles contribute more than 95% to k_b
Vagle et al. (2010)	Empirical	–	• Constrained by a least-squares fit to timeseries of near-surface-dissolved N_2 and O_2 concentration near Ocean Station Papa at the North Pacific Ocean;
Ito et al. (2011)	Empirical	–	• Constrained by fitting a global mean surface Ne saturation level of 2%.;
Nicholson et al. (2011)	Empirical	–	• Constrained by the profiles of noble gases observed at five different sites in the global ocean; • Fully dissolving bubbles contribute equally with the partially dissolved large bubbles.
Liang et al. (2013)	Physical	–	• Mechanistic model with bubble dynamics; • Designed only for the O_2 and N_2 in the ocean environment; • Fully dissolving bubbles contribute equally with the partially dissolved large bubbles.
Mischler (2014); Krall et al. (2019)	Empirical	$\propto H^{-1}$, $H \gg H_t$; $\propto Sc^{-0.5}$, $H << H_t$;	• Laboratory experiments confirm the asymptotic behavior of k_b; • Proposed a new k_b formulation; • The transition solubility was shown to be the same for the same water type in the Kyoto and SUSTAIN wind-wave tunnels and a plunging jet bubble tank.
Deike and Melville (2018); Deike et al. (2025)	Physical	$\propto H^{-0.35}Sc^{-0.5}$	• Sea state-dependent k_b parameterization based on breaking-wave physics; • The EC CO_2 and DMS data are used to constrain the coefficient of the bubble entrainment flux; • The laboratory noble gas saturation data are used to constrain the bubble-induced asymmetry for O_2.
Yang et al. (2024) Dong et al. (2025)	Empirical	–	• Developed only for k_{b_CO2} and Δ_{s_CO2} using the EC CO_2 data.

Table A9

Table A9
Selected Parameterizations of Whitecap Coverage (%) as a Function of Wind Speed

Name	Formula	Reference
Monahan 1980	$W = 3.84 \times 10^{-4} \times U_{10}{}^{3.41}$	Monahan and O'Muircheartaigh (1980)
Sugihara_07	$W = 8.04 \times 10^{-4} \times (U_{10} - 2.01)^3$	Sugihara et al. (2007)
Callaghan_08	$W = 3.18 \times 10^{-3} \times (U_{10} - 3.7)^3$	Callaghan et al. (2008)
Goddijn-M_11	$W = 15.9 \times 10^{-4} \times U_{10}{}^{2.7}$	Goddijn-Murphy et al. (2011)
Salisbury_13	$W = 4.6 \times 10^{-3} \times U_{10}{}^{2.26}$	Salisbury et al. (2013)
Scanlon_16	$W = 7.84 \times 10^{-4} \times (U_{10} - 2.56)^3$	Scanlon and Ward (2016)
Brumer_17	$W = 7.38 \times 10^{-2} \times (U_{10} - 4.23)^{1.42}$	Brumer, Zappa, Brooks, et al. (2017)

Figure A1

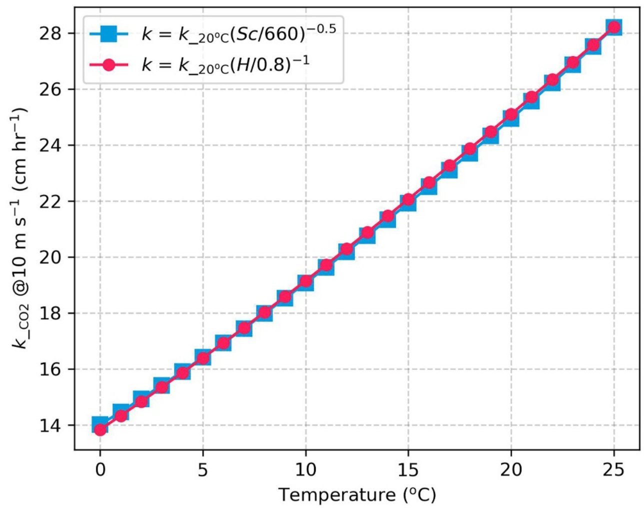

Figure A1. The temperature dependence of CO_2 transfer velocity (at 10 m s^{-1} wind speed). Blue squares represent Schmidt number (*Sc*) dependence of $k_{\_CO2}$, while red points denote solubility (*H*) dependence of $k_{\_CO2}$. The $k_{\_CO2}$ at 10 m s^{-1} wind speed is calculated from the Wanninkhof (2014) parameterization.

Figure A2

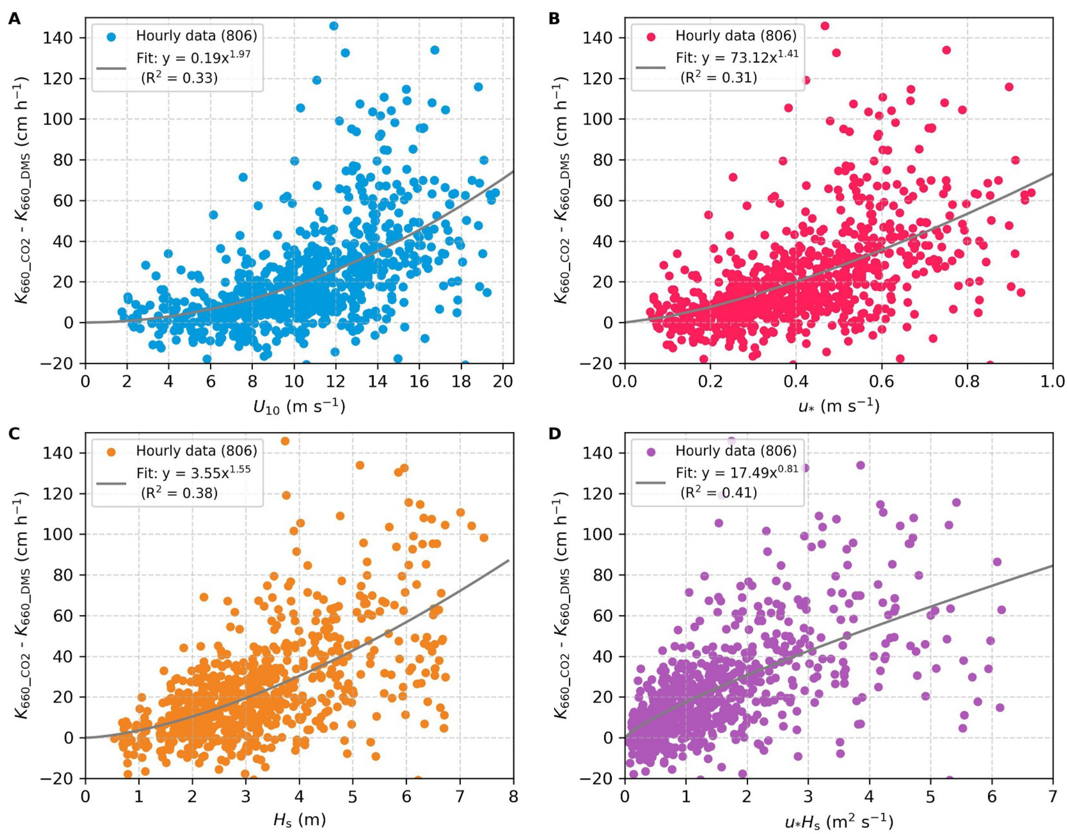

Figure A2. Difference between simultaneous CO_2 and DMS transfer velocity observations (Δk). (a) Hourly Δk versus U_{10}; (b) Hourly Δk versus friction velocity (u_*); (c) Hourly Δk versus significant wave height (H_s); (d) Hourly Δk versus u_*H_s. In each panel, the gray line shows the power-law fit ($y = ax^b$), and the R^2 for the fit is indicated in the legend of each plot.

Figure A3

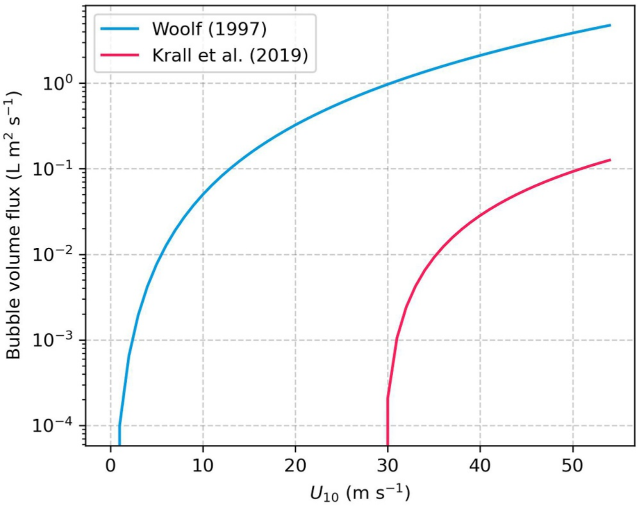

Figure A3. Bubble volume flux (V_b) from two bubble-mediated gas exchange models. The blue line represents the *Woolf_97* model, and V_b is linked with the whitecap coverage fraction based on a laboratory experiment ($V_b = 6.25$ W; Woolf, 1997). Here, W (in percentage) is calculated from a parameterization (Goddijn-Murphy et al., 2011). The red line denotes the *Krall_19* model, and V_b is inferred from the bubble-mediated transfer velocity of the relatively soluble gases (Krall et al., 2019).

Figure A4

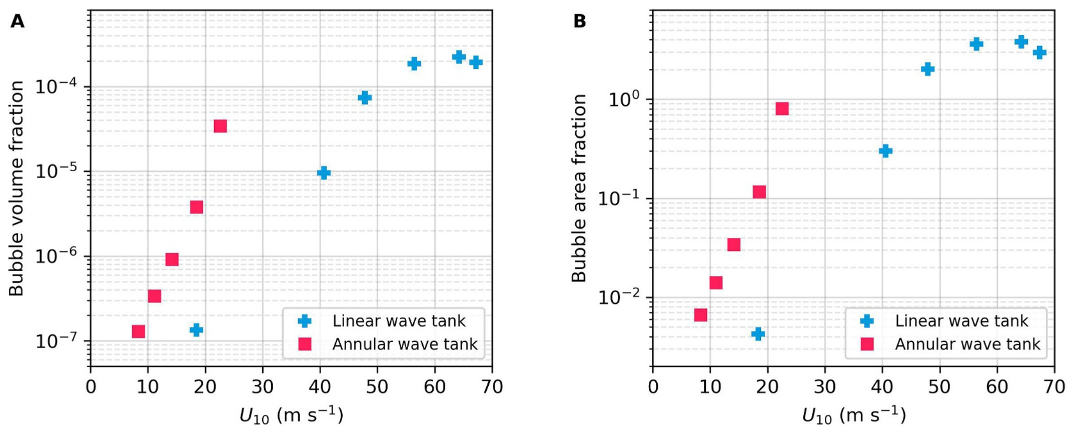

Figure A4. Void (bubble volume) fraction (left) and bubble area fraction (right) in different wind-wave tanks. All measurements were conducted approximately 30 cm beneath the surface. Blue pluses: Measurements in the linear wind-wave tank for the artificial seawater. The low wind speed results (~20 m s^{-1}) were measured in the large Marseille facility, while the high wind speed data (>40 m s^{-1}) were observed in the Kyoto facility. Red squares: Observations in an annular wind-wave tank for the artificial seawater (Aeolotron, Heidelberg University, see Table A6). Note that large uncertainties are associated with these data points due to imperfect bubble-observing techniques. Data for this figure are from Flothow (2017).

Conflict of Interest

The authors declare no conflicts of interest relevant to this study.

Availability Statement

No new data were used in this study. Figure 1 is made using PowerPoint and improved by ChatGPT. The DMS and CO_2 data shown in Figures 5 and 6, and Figure A2 are from the references summarised in Table A7. The bubble size distribution data in Figure 7 are from Deane and Stokes (2002). The modelling results in Figures A3 and 8 are available from the sources summarised in Table A8. The void fraction and bubble area fraction data in Figure A4 are from Flothow (2017). All data are reanalysed, and figures are plotted using Python. The data sources used to generate all figures are summarized in detail in the Supporting Information (SI). The Python code used to produce each figure is also provided in the Supporting Information S2.

Acknowledgments
Y. Dong has been supported by the Alexander von Humboldt Foundation. B. Jähne and K. Krall by the German Research Foundation (JA395/17-3 and JA395/19-1). D. Woolf thanks the European Space Agency for funding and support under the "Ocean Carbon for Climate" project (OC4C; 3-18399/24/I-NB). Y. Dong gratefully acknowledges Prof. T. Bell (Plymouth Marine Laboratory), Prof. P. Liss (University of East Anglia, UEA), and Prof. D. Bakker (UEA) for their insightful initial guidance on the study of air-sea gas exchange. We appreciate Prof. D. Wallace (Dalhousie University) and R. Hamme (University of Victoria) for their helpful discussion on the bubble-induced supersaturation. We thank three anonymous reviewers for their professional and valuable comments. Open Access funding enabled and organized by Projekt DEAL.

References

Asher, W. E., Karle, L. M., Higgins, B. J., Farley, P. J., Leifer, I. S., & Monahan, E. C. (1995). In B. Jahne & E. C. Monahan (Eds.), *Air-Water gas transfer* (pp. 227–238). Aeon Verlag.

Asher, W. E., Karle, L. M., Higgins, B. J., Farley, P. J., Monahan, E. C., & Leifer, I. S. (1996). The influence of bubble plumes on air-seawater gas transfer velocities. *Journal of Geophysical Research*, *101*(C5), 12027–12041. https://doi.org/10.1029/96JC00121

Asher, W. E., & Wanninkhof, R. (1998). The effect of bubble-mediated gas transfer on purposeful dual-gaseous tracer experiments. *Journal of Geophysical Research*, *103*(C5), 10555–10560. https://doi.org/10.1029/98jc00245

Atamanchuk, D., Koelling, J., Send, U., & Wallace, D. W. R. (2020). Rapid transfer of oxygen to the deep ocean mediated by bubbles. *Nature Geoscience*, *13*(3), 232–237. https://doi.org/10.1038/s41561-020-0532-2

Bange, H. W., Mongwe, P., Shutler, J. D., Arévalo-Martínez, D. L., Bianchi, D., Lauvset, S. K., et al. (2024). Advances in understanding of air-sea exchange and cycling of greenhouse gases in the upper ocean. *Elementa: Science of the Anthropocene*, *12*(1), 44. https://doi.org/10.1525/elementa.2023.00044

Banner, M. L., Zappa, C. J., & Gemmrich, J. R. (2014). A note on the Phillips spectral framework for ocean whitecaps. *Journal of Physical Oceanography*, *44*(7), 1727–1734. https://doi.org/10.1175/JPO-D-13-0126.1

Bell, T. G., De Bruyn, W., Marandino, C. A., Miller, S. D., Law, C. S., Smith, M. J., & Saltzman, E. S. (2015). Dimethylsulfide gas transfer coefficients from algal blooms in the Southern Ocean. *Atmospheric Chemistry and Physics*, *15*(4), 1783–1794. https://doi.org/10.5194/acp-15-1783-2015

Bell, T. G., De Bruyn, W., Miller, S. D., Ward, B., Christensen, K., & Saltzman, E. S. (2013). Air-sea dimethylsulfide (DMS) gas transfer in the North Atlantic: Evidence for limited interfacial gas exchange at high wind speed. *Atmospheric Chemistry and Physics*, *13*(21), 11073–11087. https://doi.org/10.5194/acp-13-11073-2013

Bell, T. G., Landwehr, S., Miller, S. D., De Bruyn, W. J., Callaghan, A. H., Scanlon, B., et al. (2017). Estimation of bubble-mediated air-sea gas exchange from concurrent DMS and CO_2 transfer velocities at intermediate-high wind speeds. *Atmospheric Chemistry and Physics*, *17*(14), 9019–9033. https://doi.org/10.5194/acp-17-9019-2017

Benetazzo, A., Halsne, T., Breivik, Ø., Strand, K. O., Callaghan, A. H., Barbariol, F., et al. (2024). On the short-term response of entrained air bubbles in the upper ocean: A case study in the north Adriatic Sea. *Ocean Science*, *20*(3), 639–660. https://doi.org/10.5194/os-20-639-2024

Blomquist, B. W., Brumer, S. E., Fairall, C. W., Huebert, B. J., Zappa, C. J., Brooks, I. M., et al. (2017). Wind speed and sea state dependencies of air-sea gas transfer: Results from the High wind Speed Gas Exchange Study (HiWinGS). *Journal of Geophysical Research: Oceans*, *122*(10), 8034–8062. https://doi.org/10.1002/2017JC013181

Blomquist, B. W., Fairall, C. W., Huebert, B. J., Kieber, D. J., & Westby, G. R. (2006). DMS sea-air transfer velocity: Direct measurements by eddy covariance and parameterization based on the NOAA/COARE gas transfer model. *Geophysical Research Letters*, *33*(7), 2–5. https://doi.org/10.1029/2006GL025735

Blomquist, B. W., Huebert, B. J., Fairall, C. W., Bariteau, L., Edson, J. B., Hare, J. E., & McGillis, W. R. (2014). Advances in air-sea CO_2 flux measurement by eddy correlation. *Boundary-Layer Meteorology*, *152*(3), 245–276. https://doi.org/10.1007/s10546-014-9926-2

Blomquist, B. W., Huebert, B. J., Fairall, C. W., & Faloona, I. C. (2010). Determining the sea-air flux of dimethylsulfide by eddy correlation using mass spectrometry. *Atmospheric Measurement Techniques*, *3*(1), 1–20. https://doi.org/10.5194/amt-3-1-2010

Bolin, B. (1960). On the exchange of carbon dioxide between the atmosphere and the sea. *Tellus*, *12*(3), 274–281. https://doi.org/10.3402/tellusa.v12i3.9402

Bowyer, P., & Woolf, D. (2004). Gas exchange and bubble-induced supersaturation in a wind-wave tank. *Journal of Atmospheric and Oceanic Technology*, *21*(12), 1925–1935. https://doi.org/10.1175/JTECH-1666.1

Broecker, H. C., & Siems, W. (1984). The role of bubbles for gas transfer from water to air at higher wind speeds. Experiments in the wind-wave facility in Hamburg. In W. Brutsaert & G. H. Jirka (Eds.), *Gas transfer at water surface* (pp. 229–238). Reidel.

Brumer, S. E., Zappa, C. J., Blomquist, B. W., Fairall, C. W., Cifuentes-Lorenzen, A., Edson, J. B., et al. (2017). Wave-related Reynolds number parameterizations of CO_2 and DMS transfer velocities. *Geophysical Research Letters*, *44*(19), 9865–9875. https://doi.org/10.1002/2017GL074979

Brumer, S. E., Zappa, C. J., Brooks, I. M., Tamura, H., Brown, S. M., Blomquist, B. W., et al. (2017). Whitecap coverage dependence on wind and wave statistics as observed during SO GasEx and HiWinGS. *Journal of Physical Oceanography*, *47*(9), 2211–2235. https://doi.org/10.1175/JPO-D-17-0005.1

Butterworth, B. J., & Miller, S. D. (2016). Air-sea exchange of carbon dioxide in the Southern Ocean and Antarctic marginal ice zone. *Geophysical Research Letters*, *43*(13), 7223–7230. https://doi.org/10.1002/2016GL069581

Callaghan, A., De Leeuw, G., Cohen, L., & O'Dowd, C. D. (2008). Relationship of oceanic whitecap coverage to wind speed and wind history. *Geophysical Research Letters*, *35*(23), 1–5. https://doi.org/10.1029/2008GL036165

Callaghan, A. H., Bidlot, J., de Leeuw, G., & O'Dowd, C. D. (2025). Comparing estimates of whitecap coverage from a spectral wave model with oceanic observations. *Geophysical Research Letters*, *52*(3), e2024GL112996. https://doi.org/10.1029/2024GL112996

Callaghan, A. H., Deane, G. B., & Stokes, M. D. (2013). Two regimes of laboratory whitecap foam decay: Bubble-plume controlled and surfactant stabilized. *Journal of Physical Oceanography*, *43*(6), 1114–1126. https://doi.org/10.1175/JPO-D-12-0148.1

Cartmill, J. W., & Su, M. Y. (1993). Bubble size distribution under saltwater and freshwater breaking waves. *Dynamics of Atmospheres and Oceans*, *20*(1–2), 25–31. https://doi.org/10.1016/0377-0265(93)90046-A

Cifuentes-Lorenzen, A., Zappa, C. J., Randolph, K., & Edson, J. B. (2023). Scaling the bubble penetration depth in the ocean. *Journal of Geophysical Research: Oceans*, *128*(9), e2022JC019582. https://doi.org/10.1029/2022JC019582

Cipriano, R. J., & Blanchard, D. C. (1981). Bubble and aerosol spectra produced by a laboratory "breaking wave.". *Journal of Geophysical Research*, *86*(C9), 8085–8092. https://doi.org/10.1029/JC086iC09p08085

Craig, H., & Hayward, T. (1987). Oxygen supersaturation in the ocean: Biological versus physical contributions. *Science*, *235*(4785), 199–202. https://doi.org/10.1126/science.235.4785.199

Craig, H., & Weiss, R. F. (1971). Dissolved gas saturation anomalies and excess helium in the ocean. *Earth and Planetary Science Letters*, *10*(3), 289–296. https://doi.org/10.1016/0012-821X(71)90033-1

Czerski, H., Brooks, I. M., Gunn, S., Pascal, R., Matei, A., & Blomquist, B. (2022a). Ocean bubbles under high wind conditions–part 1: Bubble distribution and development. *Ocean Science*, *18*(3), 565–586. https://doi.org/10.5194/os-18-565-2022

Czerski, H., Brooks, I. M., Gunn, S., Pascal, R., Matei, A., & Blomquist, B. (2022b). Ocean bubbles under high wind conditions–part 2: Bubble size distributions and implications for models of bubble dynamics. *Ocean Science*, *18*(3), 587–608. https://doi.org/10.5194/os-18-587-2022

D'Asaro, E., & McNeil, C. (2008). Air-sea gas exchange at extreme wind speeds measured by autonomous oceanographic floats. *Journal of Marine Systems*, *74*(1), 722–736. https://doi.org/10.1016/j.jmarsys.2008.02.006

Deacon, E. L. (1977). Gas transfer to and across an air-water interface. *Tellus*, *29*(4), 363–374. https://doi.org/10.3402/tellusa.v29i4.11368

Deane, G. B., & Stokes, M. D. (2002). Scale dependence of bubble creation mechanisms in breaking waves. *Nature*, *418*(6900), 839–844. https://doi.org/10.1038/nature00967

De Bruyn, W. J., & Saltzman, E. S. (1997a). Diffusivity of methyl bromide in water. *Marine Chemistry*, *57*(1–2), 55–59. https://doi.org/10.1016/S0304-4203(96)00092-8

De Bruyn, W. J., & Saltzman, E. S. (1997b). The solubility of methyl bromide in pure water, 35%. sodium chloride and seawater. *Marine Chemistry*, *56*(1–2), 51–57. https://doi.org/10.1016/S0304-4203(96)00089-8

Deike, L. (2022). Mass Transfer at the Ocean-Atmosphere Interface: The role of wave breaking, droplets, and bubbles. *Annual Review of Fluid Mechanics*, *54*(1), 191–224. https://doi.org/10.1146/annurev-fluid-030121-014132

Deike, L., & Melville, W. K. (2018). Gas transfer by breaking waves. *Geophysical Research Letters*, *45*(19), 10482–10492. https://doi.org/10.1029/2018GL078758

Deike, L., Melville, W. K., & Popinet, S. (2016). Air entrainment and bubble statistics in breaking waves. *Journal of Fluid Mechanics*, *801*, 91–129. https://doi.org/10.1017/jfm.2016.372

Deike, L., Zhou, X., Rustogi, P., Stanley, R. H. R., Reichl, B. G., Bushinsky, S. M., & Resplandy, L. (2025). A universal wind-wave- bubble formulation for air-sea gas exchange and its impact on oxygen fluxes. *Proceedings of the National Academy of Sciences*, *122*(38), e2419319122. https://doi.org/10.1073/pnas.2419319122

Doney, S. C., Lima, I., Feely, R. A., Glover, D. M., Lindsay, K., Mahowald, N., et al. (2009). Mechanisms governing interannual variability in upper-ocean inorganic carbon system and air-sea CO_2 fluxes: Physical climate and atmospheric dust. *Deep Sea Research Part II: Topical Studies in Oceanography*, *56*(8–10), 640–655. https://doi.org/10.1016/j.dsr2.2008.12.006

Doney, S. C., Wolfe, W. H., McKee, D. C., & Fuhrman, J. G. (2024). The science, engineering, and validation of marine Carbon Dioxide Removal and storage. *Annual Review of Marine Science*, *17*(1), 55–81. https://doi.org/10.1146/annurev-marine-040523-014702

Dong, Y., Bakker, D. C. E., Bell, T. G., Yang, M., Landschützer, P., Hauck, J., et al. (2024). Direct observational evidence of strong CO_2 uptake in the Southern Ocean. *Science Advances*, *10*(30), eadn5781. https://doi.org/10.1126/sciadv.adn5781

Dong, Y., Yang, M., Bakker, D. C. E., Kitidis, V., & Bell, T. G. (2021). Uncertainties in eddy covariance air-sea CO_2 flux measurements and implications for gas transfer velocity parameterisations. *Atmospheric Chemistry and Physics*, *21*(10), 8089–8110. https://doi.org/10.5194/acp-21-8089-2021

Dong, Y., Yang, M., Bakker, D. C. E., Liss, P. S., Kitidis, V., Brown, I., et al. (2021). Near-surface stratification due to ice melt biases Arctic air-sea CO_2 flux estimates. *Geophysical Research Letters*, *48*(22), 1–10. https://doi.org/10.1029/2021GL095266

Dong, Y., Yang, M., Bell, T. G., Marandino, C. A., & Woolf, D. K. (2025). Asymmetric bubble-mediated gas transfer enhances global ocean CO_2 uptake. *Nature Communications*, *16*(10595), 10595. https://doi.org/10.1038/s41467-025-66652-5

Edson, J. B., Fairall, C. W., Bariteau, L., Zappa, C. J., Cifuentes-Lorenzen, A., McGillis, W. R., et al. (2011). Direct covariance measurement of CO_2 gas transfer velocity during the 2008 Southern Ocean Gas Exchange Experiment: Wind speed dependency. *Journal of Geophysical Research*, *116*, C00F10. https://doi.org/10.1029/2011JC007022

Else, B. G. T., Papakyriakou, T. N., Galley, R. J., Drennan, W. M., Miller, L. A., & Thomas, H. (2011). Wintertime CO_2 fluxes in an Arctic polynya using eddy covariance: Evidence for enhanced air-sea gas transfer during ice formation. *Journal of Geophysical Research*, *116*, C00G03. https://doi.org/10.1029/2010JC006760

Emerson, S., & Bushinsky, S. (2016). The role of bubbles during air-sea gas exchange. *Journal of Geophysical Research: Oceans*, *121*(6), 4360–4376. https://doi.org/10.1002/2016JC011744

Emerson, S., Yang, B., White, M., & Cronin, M. (2019). Air-sea gas transfer: Determining bubble fluxes with in situ N_2 observations. *Journal of Geophysical Research: Oceans*, *124*(4), 2716–2727. https://doi.org/10.1029/2018JC014786

Fairall, C. W., Yang, M., Bariteau, L., Edson, J. B., Helmig, D., McGillis, W., et al. (2011). Implementation of the Coupled Ocean-Atmosphere Response Experiment flux algorithm with CO_2, dimethyl sulfide, and O_3. *Journal of Geophysical Research*, *116*(10), C00F09. https://doi.org/10.1029/2010JC006884

Fairall, C. W., Yang, M., Brumer, S. E., Blomquist, B. W., Edson, J. B., Zappa, C. J., et al. (2022). Air-sea trace gas fluxes: Direct and indirect measurements. *Frontiers in Marine Science*, *9*(July), 1–16. https://doi.org/10.3389/fmars.2022.826606

Farmer, D. M., McNeil, C. L., & Johnson, B. D. (1993). Evidence for the importance of bubbles in increasing air-sea gas flux. *Nature*, *361*(6413), 620–623. https://doi.org/10.1038/361620a0

Flothow, L. (2017). Bubble characteristics from breaking waves in fresh water and simulated seawater Master's thesis. Institut für Umweltphysik. https://doi.org/10.11588/heidok.00023754

Ford, D. J., Shutler, J. D., Blanco-Sacristán, J., Corrigan, S., Bell, T. G., Yang, M., et al. (2024). Enhanced ocean CO_2 uptake due to near-surface temperature gradients. *Nature Geoscience*, *17*(11), 1135–1140. https://doi.org/10.1038/s41561-024-01570-7

Friedlingstein, P., O'Sullivan, M., Jones, M. W., Andrew, R. M., Hauck, J., Landschützer, P., et al. (2025). Global Carbon Budget 2024. *Earth System Science Data*, *17*(3), 965–1039. https://doi.org/10.5194/essd-17-965-2025

Garbe, C. S., Rutgersson, A., Boutin, J., De Leeuw, G., Delille, B., Fairall, C. W., et al. (2014). Transfer across the air-sea interface. In *Ocean-atmosphere interactions of gases and particles* (pp. 55–112). Springer.

Goddijn-Murphy, L., Woolf, D. K., & Callaghan, A. H. (2011). Parameterizations and algorithms for oceanic whitecap coverage. *Journal of Physical Oceanography*, *41*(4), 742–756. https://doi.org/10.1175/2010JPO4533.1

Goddijn-Murphy, L., Woolf, D. K., Callaghan, A. H., Nightingale, P. D., & Shutler, J. D. (2016). A reconciliation of empirical and mechanistic models of the air-sea gas transfer velocity. *Journal of Geophysical Research: Oceans*, *121*(1), 818–835. https://doi.org/10.1002/2015JC011096

Graham, A., Woolf, D. K., & Hall, A. J. (2004). Aeration due to breaking waves. Part I: Bubble populations. *Journal of Physical Oceanography*, *34*(5), 989–1007. https://doi.org/10.1175/1520-0485(2004)034<0989:ADTBWP>2.0.CO;2

Hamme, R. C., & Emerson, S. R. (2002). Mechanisms controlling the global oceanic distribution of the inert gases argon, nitrogen and neon. *Geophysical Research Letters*, *29*(23), 31–35. https://doi.org/10.1029/2002GL015273

Hamme, R. C., & Emerson, S. R. (2006). Constraining bubble dynamics and mixing with dissolved gases: Implications for productivity measurements by oxygen mass balance. *Journal of Marine Research*, *64*(1), 73–95. https://doi.org/10.1357/002224006776412322

Hamme, R. C., Emerson, S. R., Severinghaus, J. P., Long, M. C., & Yashayaev, I. (2017). Using noble gas measurements to derive air-sea process information and predict physical gas saturations. *Geophysical Research Letters*, *44*(19), 9901–9909. https://doi.org/10.1002/2017GL075123

Hinze, J. O. (1955). Fundamentals of the hydrodynamic mechanism of splitting in dispersion processes. *AIChE Journal*, *1*(3), 289–295. https://doi.org/10.1002/aic.690010303

Ho, D. T., Law, C. S., Smith, M. J., Schlosser, P., Harvey, M., & Hill, P. (2006). Measurements of air-sea gas exchange at high wind speeds in the Southern Ocean: Implications for global parameterizations. *Geophysical Research Letters*, *33*(16). https://doi.org/10.1029/2006GL026817

Huebert, B. J., Blomquist, B. W., Hare, J. E., Fairall, C. W., Johnson, J. E., & Bates, T. S. (2004). Measurement of the sea-air DMS flux and transfer velocity using eddy correlation. *Geophysical Research Letters*, *31*(23), 1–4. https://doi.org/10.1029/2004GL021567

Huebert, B. J., Blomquist, B. W., Yang, M. X., Archer, S. D., Nightingale, P. D., Yelland, M. J., et al. (2010). Speeds up to 85 m s-1. Ocean Science, 15(6),friction velocity and wind speed in the moderate wind speed range. *Geophysical Research Letters*, *37*(1). https://doi.org/10.1029/2009GL041203

Ito, T., Hamme, R. C., & Emerson, S. (2011). Temporal and spatial variability of noble gas tracers in the North Pacific. *Journal of Geophysical Research*, *116*(C8), C08039. https://doi.org/10.1029/2010JC006828

Iwano, K., Takagaki, N., Kurose, R., & Komori, S. (2013). Mass transfer velocity across the breaking air-water interface at extremely high wind speeds. *Tellus Series B Chemical and Physical Meteorology*, *65*(1), 21341. https://doi.org/10.3402/tellusb.v65i0.21341

Jacobs, C., Friis Kjeld, J., Nightingale, P., Upstill-Goddard, R., Larsen, S., & Oost, W. (2002). Possible errors in CO_2 air-sea transfer velocity from deliberate tracer releases and eddy covariance measurements due to near-surface concentration gradients. *Journal of Geophysical Research*, *107*(C9), 11. https://doi.org/10.1029/2001JC000983

Jähne, B., Heinz, G., & Dietrich, W. (1987). Measurement of the diffusion coefficients of sparingly soluble gases in water. *Journal of Geophysical Research*, *92*(C10), 10767–10776. https://doi.org/10.1029/JC092iC10p10767

Jähne, B., Wais, T., & Barabas, M. (1984). A new optical bubble measuring device; a simple model for bubble contribution to gas exchange. In W. Brutsaert & G. H. Jirka (Eds.), *Gas transfer at water surfaces* (pp. 237–246). Springer Netherlands. https://doi.org/10.1007/978-94-017-1660-4_22

Jenkins, W. J., Lott III, D. E., & Cahill, K. L. (2019). A determination of atmospheric helium, neon, argon, krypton, and xenon solubility concentrations in water and seawater. *Marine Chemistry*, *211*, 94–107. https://doi.org/10.1016/j.marchem.2019.03.007

Kanwisher, J. (1963). On the exchange of gases between the atmosphere and the sea. *Deep-Sea Research and Oceanographic Abstracts*, *10*(3), 195–207. https://doi.org/10.1016/0011-7471(63)90356-5

Keeling, R. F. (1993). On the role of large bubbles in air-sea gas exchange and supersaturation in the ocean. *Journal of Marine Research*, *51*(2), 237–271. https://doi.org/10.1357/0022240933223800

Koelling, J., Wallace, D. W. R., Send, U., & Karstensen, J. (2017). Intense oceanic uptake of oxygen during 2014–2015 winter convection in the Labrador Sea. *Geophysical Research Letters*, *44*(15), 7855–7864. https://doi.org/10.1002/2017GL073933

Kondo, F., & Tsukamoto, O. (2007). Air-sea CO_2 flux by eddy covariance technique in the equatorial Indian Ocean. *Journal of Oceanography*, *63*(3), 449–456. https://doi.org/10.1007/s10872-007-0040-7

Krall, K. E., & Jähne, B. (2014). First laboratory study of air-sea gas exchange at hurricane wind speeds. *Ocean Science*, *10*(2), 257–265. https://doi.org/10.5194/os-10-257-2014

Krall, K. E., Smith, A. W., Takagaki, N., & Jähne, B. (2019). Air-sea gas exchange at wind speeds up to 85 m s^{-1}. *Ocean Science*, *15*(6), 1783–1799. https://doi.org/10.5194/os-15-1783-2019

Landwehr, S., Miller, S. D., Smith, M. J., Bell, T. G., Saltzman, E. S., & Ward, B. (2018). Using eddy covariance to measure the dependence of air-sea CO_2 exchange rate on friction velocity. *Atmospheric Chemistry and Physics*, *18*(6), 4297–4315. https://doi.org/10.5194/acp-18-4297-2018

Landwehr, S., Miller, S. D., Smith, M. J., Saltzman, E. S., & Ward, B. (2014). Analysis of the PKT correction for direct CO_2 flux measurements over the ocean. *Atmospheric Chemistry and Physics*, *14*(7), 3361–3372. https://doi.org/10.5194/acp-14-3361-2014

Lauvset, S. K., McGillis, W. R., Bariteau, L., Fairall, C. W., Johannessen, T., Olsen, A., & Zappa, C. J. (2011). Direct measurements of CO_2 flux in the Greenland Sea. *Geophysical Research Letters*, *38*(12). https://doi.org/10.1029/2011GL047722

Lee, H., Calvin, K., Dasgupta, D., Krinner, G., Mukherji, A., Thorne, P., et al. (2023). *Climate change 2023: Synthesis report. Contribution of working groups I, II and III to the sixth assessment report of the intergovernmental Panel on climate change*. IPCC.

Leifer, I. S., Asher, W. E., & Farley, P. J. (1995). A validation study of bubble mediated air-sea gas transfer modeling for trace gases. In *Selected papers from the third international symposium on air-water gas transfer* (pp. 269–283).

Leighton, T. G., Coles, D. G. H., Srokosz, M., White, P. R., & Woolf, D. K. (2018). Asymmetric transfer of CO_2 across a broken sea surface. *Scientific Reports*, *8*(1), 1–9. https://doi.org/10.1038/s41598-018-25818-6

Levich, V. G. (1962). *Physico-chemical hydrodynamics*. Prentice Hall.700pp.

Liang, J., McWilliams, J. C., Sullivan, P. P., & Baschek, B. (2011). Modeling bubbles and dissolved gases in the ocean. *Journal of Geophysical Research*, *116*(C3), C03015. https://doi.org/10.1029/2010JC006579

Liang, J., McWilliams, J. C., Sullivan, P. P., & Baschek, B. (2012). Large eddy simulation of the bubbly ocean: New insights on subsurface bubble distribution and bubble-mediated gas transfer. *Journal of Geophysical Research*, *117*(C4). https://doi.org/10.1029/2011JC007766

Liang, J. H., Deutsch, C., McWilliams, J. C., Baschek, B., Sullivan, P. P., & Chiba, D. (2013). Parameterizing bubble-mediated air-sea gas exchange and its effect on ocean ventilation. *Global Biogeochemical Cycles*, *27*(3), 894–905. https://doi.org/10.1002/gbc.20080

Liss, P. S., & Slater, P. G. (1974). Flux of gases across the air-sea interface. *Nature*, *247*(5438), 181–184. https://doi.org/10.1038/247181a0

Marandino, C. A., De Bruyn, W. J., Miller, S. D., & Saltzman, E. S. (2007). Eddy correlation measurements of the air/sea flux of dimethylsulfide over the North Pacific Ocean. *Journal of Geophysical Research*, *112*(D3). https://doi.org/10.1029/2006JD007293

Marandino, C. A., De Bruyn, W. J., Miller, S. D., & Saltzman, E. S. (2008). DMS air/sea flux and gas transfer coefficients from the North Atlantic summertime coccolithophore bloom. *Geophysical Research Letters*, *35*(23), 1–5. https://doi.org/10.1029/2008GL036370

Marandino, C. A., De Bruyn, W. J., Miller, S. D., & Saltzman, E. S. (2009). Open ocean DMS air/sea fluxes over the eastern South Pacific Ocean. *Atmospheric Chemistry and Physics*, *9*(2), 345–356. https://doi.org/10.5194/acp-9-345-2009

McGillis, W. R., Bock, E. J., & Frew, N. M. (1995). Mass transfer from gas bubbles in fresh and seawater. In B. Jähne & E. C. Monahan (Eds.), *In air-water gas transfer* (pp. 363–374). Aeon Verlag.

McGillis, W. R., Edson, J. B., Ware, J. D., Dacey, J. W. H., Hare, J. E., Fairall, C. W., & Wanninkhof, R. (2001). Carbon dioxide flux techniques performed during GasEx-98. *Marine Chemistry*, *75*(4), 267–280. https://doi.org/10.1016/S0304-4203(01)00042-1

McGillis, W. R., Edson, J. B., Zappa, C. J., Ware, J. D., McKenna, S. P., Terray, E. A., et al. (2004). Air-sea CO_2 exchange in the equatorial Pacific. *Journal of Geophysical Research*, *109*(C8). https://doi.org/10.1029/2003JC002256

McNeil, C., & D'Asaro, E. (2007). Parameterization of air-sea gas fluxes at extreme wind speeds. *Journal of Marine Systems*, *66*(1–4), 110–121. https://doi.org/10.1016/j.jmarsys.2006.05.013

Medwin, H., & Breitz, N. D. (1989). Ambient and transient bubble spectral densities in Quiescent Seas and under spilling breakers. *Journal of Geophysical Research*, *94*(C9), 751–759. https://doi.org/10.1029/JC094iC09p12751

Memery, L., & Merlivat, L. (1984). Contribution of bubbles to gas transfer across an air-water interface. In *Gas transfer at water surfaces* (pp. 247–253). Springer.

Memery, L., & Merlivat, L. (1985). Modelling of gas flux through bubbles at the air-water interface. *Tellus B: Chemical and Physical Meteorology*, *37*(4–5), 272–285. https://doi.org/10.3402/tellusb.v37i4-5.15030

Merlivat, L., & Memery, L. (1983). Gas exchange across an air-water interface: Experimental results and modeling of bubble contribution to transfer. *Journal of Geophysical Research*, *88*(C1), 707–724. https://doi.org/10.1029/JC088iC01p00707

Mesarchaki, E., Kräuter, C., Krall, K. E., Bopp, M., Helleis, F., Williams, J., & Jähne, B. (2015). Measuring air-sea gas-exchange velocities in a large-scale annular wind-wave tank. *Ocean Science*, *11*(1), 121–138. https://doi.org/10.5194/os-11-121-2015

Miller, S., Marandino, C. A., De Bruyn, W., & Saltzman, E. S. (2009). Air-sea gas exchange of CO_2 and DMS in the North Atlantic by eddy covariance. *Geophysical Research Letters*, *36*(15), 1–5. https://doi.org/10.1029/2009GL038907

Miller, S. D., Marandino, C. A., & Saltzman, E. S. (2010). Ship-based measurement of air-sea CO_2 exchange by eddy covariance. *Journal of Geophysical Research*, *115*(D2), 1–14. https://doi.org/10.1029/2009JD012193

Mischler, W. (2014). *Systematic measurements of bubble induced gas exchange for trace gases with low solubilities, Dissertation, Institut für Umweltphysik, Fakultät für Physik und Astronomie*. Univ.Heidelberg. https://doi.org/10.11588/heidok.00017720

Monahan, E. C., & Lu, M. (1990). Acoustically relevant bubble assemblages and their dependence on meteorological parameters. *IEEE Journal of Oceanic Engineering*, *15*(4), 340–349. https://doi.org/10.1109/48.103530

Monahan, E. C., & O'Muircheartaigh, I. (1980). Optimal power-law description of oceanic whitecap coverage dependence on wind speed. *Journal of Physical Oceanography*, *10*(12), 2094–2099. https://doi.org/10.1175/1520-0485(1980)010<2094:OPLDOO>2.0.CO;2

Monahan, E. C., & O'Muircheartaigh, I. G. (1986). Whitecaps and the passive remote sensing of the ocean surface. *International Journal of Remote Sensing*, *7*(5), 627–642. https://doi.org/10.1080/01431168608954716

Monahan, E. C., & Mac Niocaill, G. (1986). *Oceanic whitecaps: And their role in air-sea exchange processes* (Vol. 2). Springer Science and Business Media. https://doi.org/10.1007/978-94-009-4668-2

Nicholson, D. P., Emerson, S. R., & Khatiwala, S. (2011). An inverse approach to estimate bubble-mediated air-sea gas flux from inert gas measurements. In *Proceedings on the 6th international symposium on gas transfer at water surfaces* (pp. 223–237). Kyoto Univ. Press.

Nilsson, E., Bergström, H., Rutgersson, A., Podgrajsek, E., Wallin, M. B., Bergström, G., et al. (2018). Evaluating humidity and sea salt disturbances on CO_2 flux measurements. *Journal of Atmospheric and Oceanic Technology*, *35*(4), 859–875. https://doi.org/10.1175/JTECH-D-17-0072.1

Phillips, O. M. (1985). Spectral and statistical properties of the equilibrium range in wind-generated gravity waves. *Journal of Fluid Mechanics*, *156*, 505–531. https://doi.org/10.1017/s0022112085002221

Pierson, W. J., Jr., & Moskowitz, L. (1964). A proposed spectral form for fully developed wind seas based on the similarity theory of SA Kitaigorodskii. *Journal of Geophysical Research*, *69*(24), 5181–5190. https://doi.org/10.1029/JZ069i024p05181

Powell, M. D., Vickery, P. J., & Reinhold, T. A. (2003). Reduced drag coefficient for high wind speeds in tropical cyclones. *Nature*, *422*(6929), 279–283. https://doi.org/10.1038/nature01481

Prytherch, J., Yelland, M. J., Pascal, R. W., Moat, B. I., Skjelvan, I., & Neill, C. C. (2010). Direct measurements of the CO_2 flux over the ocean: Development of a novel method. *Geophysical Research Letters*, *37*(3). https://doi.org/10.1029/2009GL041482

Reichl, B. G., & Deike, L. (2020). Contribution of sea-state dependent bubbles to air-sea carbon dioxide fluxes. *Geophysical Research Letters*, *47*(9), e2020GL087267. https://doi.org/10.1029/2020GL087267

Rhee, T. S., Nightingale, P. D., Woolf, D. K., Caulliez, G., Bowyer, P., & Andreae, M. O. (2007). Influence of energetic wind and waves on gas transfer in a large wind-wave tunnel facility. *Journal of Geophysical Research*, *112*(5), 1–16. https://doi.org/10.1029/2005JC003358

Rustogi, P., Resplandy, L., Liao, E., Reichl, B. G., & Deike, L. (2025). Influence of wave-induced variability on ocean carbon uptake. *Global Biogeochemical Cycles*, *39*(6), e2024GB008382. https://doi.org/10.1029/2024GB008382

Ruth, D. J., Aiyer, A. K., Rivière, A., Perrard, S., & Deike, L. (2022). Experimental observations and modelling of sub-hinze bubble production by turbulent bubble break-up. *Journal of Fluid Mechanics*, *951*, A32. https://doi.org/10.1017/jfm.2022.604

Ruth, D. J., Vernet, M., Perrard, S., & Deike, L. (2021). The effect of nonlinear drag on the rise velocity of bubbles in turbulence. *Journal of Fluid Mechanics*, *924*, A2. https://doi.org/10.1017/jfm.2021.556

Salibindla, A. K., Masuk, A. U. M., Tan, S., & Ni, R. (2020). Lift and drag coefficients of deformable bubbles in intense turbulence determined from bubble rise velocity. *Journal of Fluid Mechanics*, *894*, A20. https://doi.org/10.1017/jfm.2020.244

Salisbury, D. J., Anguelova, M. D., & Brooks, I. M. (2013). On the variability of whitecap fraction using satellite-based observations. *Journal of Geophysical Research: Oceans*, *118*(11), 6201–6222. https://doi.org/10.1002/2013JC008797

Salter, M. E., Upstill-Goddard, R. C., Nightingale, P. D., Archer, S. D., Blomquist, B., Ho, D. T., et al. (2011). Impact of an artificial surfactant release on air-sea gas fluxes during Deep Ocean Gas Exchange Experiment II. *Journal of Geophysical Research*, *116*(C11). https://doi.org/10.1029/2011JC007023

Sander, R. (2023). Compilation of Henry's law constants (version 5.0.0) for water as solvent. *Atmospheric Chemistry and Physics*, *23*(19), 10901–12440. https://doi.org/10.5194/acp-23-10901-2023

Scanlon, B., & Ward, B. (2016). The influence of environmental parameters on active and maturing oceanic whitecaps. *Journal of Geophysical Research: Oceans*, *121*(5), 3325–3336. https://doi.org/10.1002/2015JC011230

Seltzer, A. M., Nicholson, D. P., Smethie, W. M., Tyne, R. L., Le Roy, E., Stanley, R. H. R., et al. (2023). Dissolved gases in the deep North Atlantic track ocean ventilation processes. *Proceedings of the National Academy of Sciences*, *120*(11), e2217946120. https://doi.org/10.1073/pnas.2217946120

Spitzer, W. S., & Jenkins, W. J. (1989). Rates of vertical mixing, gas exchange and new production: Estimates from seasonal gas cycles in the upper ocean near Bermuda. *Journal of Marine Research*, *47*(1), 169–196. https://doi.org/10.1357/002224089785076370

Stanley, R. H. R., & Bell, T. G. (2025). *Air-sea gas exchange and marine gases*. In A. Anbar & D. B. (Eds.) (pp. 53–83). Elsevier. https://doi.org/10.1016/B978-0-323-99762-1.00055-3

Stanley, R. H. R., Jenkins, W. J., & Doney, S. C. (2006). Quantifying seasonal air-sea gas exchange processes using noble gas time-series: A design experiment. *Journal of Marine Research*, *64*(2), 267–295. https://doi.org/10.1357/002224006777606452

Stanley, R. H. R., Jenkins, W. J., Lott, D. E., & Doney, S. C. (2009). Noble gas constraints on air-sea gas exchange and bubble fluxes. *Journal of Geophysical Research*, *114*(11), 1–14. https://doi.org/10.1029/2009JC005396

Stanley, R. H. R., Kinjo, L., Smith, A. W., Aldrett, D., Alt, H., Kopp, E., et al. (2022). Gas fluxes and steady State saturation anomalies at very high wind speeds. *Journal of Geophysical Research: Oceans*, *127*(10), 1–19. https://doi.org/10.1029/2021jc018387

Sugihara, Y., Tsumori, H., Ohga, T., Yoshioka, H., & Serizawa, S. (2007). Variation of whitecap coverage with wave-field conditions. *Journal of Marine Systems*, *66*(1–4), 47–60. https://doi.org/10.1016/j.jmarsys.2006.01.014

Sullivan, P. P., & McWilliams, J. C. (2010). Dynamics of winds and currents coupled to surface waves. *Annual Review of Fluid Mechanics*, *42*(1), 19–42. https://doi.org/10.1146/annurev-fluid-121108-145541

Sun, H., Zheng, K., Yu, J., & Zheng, H. (2023). Spatiotemporal distributions of air-sea CO_2 flux modulated by windseas in the Southern Indian Ocean. *Frontiers in Marine Science*, *10*, 1139591. https://doi.org/10.3389/fmars.2023.1139591

Sutherland, P., & Melville, W. K. (2013). Field measurements and scaling of ocean surface wave-breaking statistics. *Geophysical Research Letters*, *40*(12), 3074–3079. https://doi.org/10.1002/grl.50584

Takagaki, N., Komori, S., Suzuki, N., Iwano, K., Kuramoto, T., Shimada, S., et al. (2012). Strong correlation between the drag coefficient and the shape of the wind sea spectrum over a broad range of wind speeds. *Geophysical Research Letters*, *39*(23), 1–6. https://doi.org/10.1029/2012GL053988

Terray, E. A., Donelan, M. A., Agrawal, Y. C., Drennan, W. M., Kahma, K. K., Williams, A. J., et al. (1996). Estimates of kinetic energy dissipation under breaking waves. *Journal of Physical Oceanography*, *26*(5), 792–807. https://doi.org/10.1175/1520-0485(1996)026<0792:EOKEDU>2.0.CO;2

Thorpe, S. A. (1984a). The effect of Langmuir circulation on the distribution of submerged bubbles caused by breaking wind waves. *Journal of Fluid Mechanics*, *142*(C7), 151–170. https://doi.org/10.1017/S0022112084001038

Thorpe, S. A. (1984b). A model of the turbulent diffusion of bubbles below the sea surface. *Journal of Physical Oceanography*, *14*(5), 841–854. https://doi.org/10.1175/1520-0485(1984)014<0841:amottd>2.0.co;2

Thorpe, S. A. (2004). Langmuir circulation. *Annual Review of Fluid Mechanics*, *36*(1), 55–79. https://doi.org/10.1146/annurev.fluid.36.052203.071431

Thorpe, S. A., Bowyer, P., & Woolf, D. K. (1992). Some factors affecting the size distributions of oceanic bubbles. *Journal of Physical Oceanography*, *22*(4), 382–389. https://doi.org/10.1175/1520-0485(1992)022<0382:SFATSD>2.0.CO;2

Ulses, C., Estournel, C., Fourrier, M., Coppola, L., Kessouri, F., Lefèvre, D., & Marsaleix, P. (2021). Oxygen budget of the north-western Mediterranean deep-convection region. *Biogeosciences*, *18*(3), 937–960. https://doi.org/10.5194/bg-18-937-2021

Vagle, S., McNeil, C., & Steiner, N. (2010). Upper ocean bubble measurements from the NE Pacific and estimates of their role in air-sea gas transfer of the weakly soluble gases nitrogen and oxygen. *Journal of Geophysical Research*, *115*(12), 1–16. https://doi.org/10.1029/2009JC005990

Vassilicos, J. C. (2015). Dissipation in turbulent flows. *Annual Review of Fluid Mechanics*, *47*(1), 95–114. https://doi.org/10.1146/annurev-fluid-010814-014637

Vlahos, P., & Monahan, E. C. (2009). A generalized model for the air-sea transfer of dimethyl sulfide at high wind speeds. *Geophysical Research Letters*, *36*(21), 1–6. https://doi.org/10.1029/2009GL040695

Wallace, D. W. R., & Wirick, C. D. (1992). Large air-sea gas fluxes associated with breaking waves. *Nature*, *356*(6371), 694–696. https://doi.org/10.1038/356694a0

Wang, Q., Monahan, E. C., Asher, W. E., & Smith, P. M. (1995). Correlations of whitecap coverage and gas transfer velocity with microwave brightness temperature for plunging and spilling breaking waves. In *Selected papers from the third international symposium on air-water gas transfer* (pp. 217–226).

Wanninkhof, R. (1992). Relationship between wind speed and gas exchange over the ocean. *Journal of Geophysical Research*, *97*(C5), 7373–7382. https://doi.org/10.1029/92jc00188

Wanninkhof, R. (2014). Relationship between wind speed and gas exchange over the ocean revisited. *Limnology and Oceanography: Methods*, *12*(6), 351–362. https://doi.org/10.4319/lom.2014.12.351

Wanninkhof, R., Asher, W., & Monahan, E. (1995). The influence of bubbles on air-water gas exchange: Results from gas transfer experiments during WABEX-93. In *Selected papers from the third international symposium on air-water gas transfer* (pp. 239–253).

Wanninkhof, R., Asher, W. E., Ho, D. T., Sweeney, C., & McGillis, W. R. (2009). Advances in quantifying air-sea gas exchange and environmental forcing. *Annual Review of Marine Science*, *1*(1), 213–244. https://doi.org/10.1146/annurev.marine.010908.163742

Woolf, D. (2025). Eight categories of air-water gas transfer. In *Oceans*, (Vol. 6(2)), 27. MDPI. https://doi.org/10.3390/oceans6020027

Woolf, D. K. (1993). Bubbles and the air-sea transfer velocity of gases. *Atmosphere-Ocean*, *31*(4), 517–540. https://doi.org/10.1080/07055900.1993.9649484

Woolf, D. K. (1997). Bubbles and their role in gas exchange. In P. S. Liss & R. A. Duce (Eds.), *The Sea surface and global change* (pp. 173–206). Cambridge Univ. Press.

Woolf, D. K. (2005). Parametrization of gas transfer velocities and sea-state-dependent wave breaking. *Tellus B: Chemical and Physical Meteorology*, *57*(2), 87. https://doi.org/10.3402/tellusb.v57i2.16783

Woolf, D. K., Leifer, I. S., Nightingale, P. D., Rhee, T. S., Bowyer, P., Caulliez, G., et al. (2007). Modelling of bubble-mediated gas transfer: Fundamental principles and a laboratory test. *Journal of Marine Systems*, *66*(1–4), 71–91. https://doi.org/10.1016/j.jmarsys.2006.02.011

Woolf, D. K., & Thorpe, S. A. (1991). Bubbles and the air-sea exchange of gases in near-saturation conditions. *Journal of Marine Research*, *49*(3), 435–466. https://doi.org/10.1357/002224091784995765

Wurl, O., Wurl, E., Miller, L., Johnson, K., & Vagle, S. (2011). Formation and global distribution of sea-surface microlayers. *Biogeosciences*, *8*(1), 121–135. https://doi.org/10.5194/bg-8-121-2011

Yang, B., Emerson, S. R., & Bushinsky, S. M. (2017). Annual net community production in the subtropical Pacific Ocean from in situ oxygen measurements on profiling floats. *Global Biogeochemical Cycles*, *31*(4), 728–744. https://doi.org/10.1002/2016GB005545

Yang, M., Bell, T. G., Bidlot, J. R., Blomquist, B. W., Butterworth, B. J., Dong, Y., et al. (2022). Global synthesis of air-sea CO_2 transfer velocity estimates from ship-based eddy covariance measurements. *Frontiers in Marine Science*, *9*(June), 1–15. https://doi.org/10.3389/fmars.2022.826421

Yang, M., Blomquist, B. W., Fairall, C. W., Archer, S. D., & Huebert, B. J. (2011). Air-sea exchange of dimethylsulfide in the Southern Ocean: Measurements from SO GasEx compared to temperate and tropical regions. *Journal of Geophysical Research*, *116*(8), 1–17. https://doi.org/10.1029/2010JC006526

Yang, M., Blomquist, B. W., & Huebert, B. J. (2009). Constraining the concentration of the hydroxyl radical in a stratocumulus-topped marine boundary layer from sea-to-air eddy covariance flux measurements of dimethylsulfide. *Atmospheric Chemistry and Physics*, *9*(23), 9225–9236. https://doi.org/10.5194/acp-9-9225-2009

Yang, M., Moffat, D., Dong, Y., & Bidlot, J.-R. (2024). Deciphering the variability in air-sea gas transfer due to sea state and wind history. *PNAS Nexus*, *3*(9), pgae389. https://doi.org/10.1093/pnasnexus/pgae389

Yang, M., Smyth, T. J., Kitidis, V., Brown, I. J., Wohl, C., Yelland, M. J., & Bell, T. G. (2021). Natural variability in air-sea gas transfer efficiency of CO_2. *Scientific Reports*, *11*(1), 1–9. https://doi.org/10.1038/s41598-021-92947-w

Yaws, C. L. (2009). Diffusion coefficient in water-inorganic compounds. In *Transport properties of chemicals and hydrocarbons* (pp. 594–596). Elsevier. https://doi.org/10.1016/B978-0-8155-2039-9.50018-1

Zavarsky, A., Goddijn-Murphy, L., Steinhoff, T., & Marandino, C. A. (2018). Bubble-mediated gas transfer and gas transfer suppression of DMS and CO_2. *Journal of Geophysical Research: Atmospheres*, *123*(12), 6624–6647. https://doi.org/10.1029/2017JD028071

Zhang, X. (2012). Contribution to the global air-sea CO_2 exchange budget from asymmetric bubble-mediated gas transfer. *Tellus Series B Chemical and Physical Meteorology*, *64*(1), 17260. https://doi.org/10.3402/tellusb.v64i0.17260

Zhao, D., Toba, Y., Suzuki, Y., & Komori, S. (2003). Effect of wind waves on air-sea gas exchange: Proposal of an overall CO_2 transfer velocity formula as a function of breaking-wave parameter. *Tellus B: Chemical and Physical Meteorology*, *55*(2), 478–487. https://doi.org/10.3402/tellusb.v55i2.16747

Zhou, X., Reichl, B. G., Romero, L., & Deike, L. (2023). A sea state dependent gas transfer velocity for CO_2 unifying theory, model, and field data. *Earth and Space Science*, *10*(11), e2023EA003237. https://doi.org/10.1029/2023EA003237